A SYSTEM FOR ESTIMATING WATER CONTENT OF CONIFER FORESTS USING HYPERSPECTRAL REMOTE SENSING DATA

by

Jing Yang Li

M.Sc. in Meteorology, Chinese Academy of Sciences, China, 1999
B.Sc. in Meteorology, Nanjing University, China, 1990

A Thesis Submitted in Partial Fulfillment of the
Requirements for the Degree of

MASTER of SCIENCE

In the Department of Computer Science

Supervisor: Dr. David G. Goodenough

Abstract

Estimation of foliage water content from remote sensing data is critical to wildfire management and monitoring forest health. Several efforts to estimate vegetation water content have relied on empirical relationships and data-specific calibrations. Therefore, the approaches used by these studies are not applicable to larger scales and different species. This work was undertaken to develop systems for retrieving foliage water content of Douglas-fir stands with closed canopy. The canopy structural parameters were constrained by forest dynamic relationships. Sensitivity analysis was used to quantify the influence of foliage water content and other factors (LAI, canopy closure, soil) on canopy reflectance simulated in the spectral range between 400 and 2400 nm. Lookup tables were generated using a forest radiative transfer model. Fuel moisture content (FMC) of Douglas-fir can then be determined from airborne hyperspectral imagery (AVIRIS) by the lookup table method. We achieved an accuracy of R^2 of 0.74 for FMC which was assessed through comparisons of the estimated foliage water content with field measurements. A software system, FMAS (Fuel Moisture Content Mapping System), was developed for the estimation of fuel moisture content of Douglas-fir forests. Conclusions and further research issues were discussed.

Examiners:

Dr. David G. Goodenough, Supervisor (Department of Computer Science)

Dr. Wendy Myrvold, Departmental Member (Department of Computer Science)

Dr. K. Olaf Niemann, External Member (Department of Geography)

Dr. Harold Zwick, Outside Examiner (MacDonald Dettwiler)

TABLE OF CONTENTS

List of Acronyms

ASAS	Advanced Solid-State Array Spectroradiometer
ASD	Analytical Spectral Devices
AVHRR	Advanced Very High Resolution Radiometer
AVIRIS	Airborne Visible and Infrared Imaging Spectrometer
BAI	Branch Area Index (cm^2/cm^2)
CASI	Compact Airborne Spectrographic Imager
CFFDRS	Canadian Forest Fire Danger Rating System
DBH	Diameter at Breast Height (cm)
DM	Dry matter content (g/cm^2)
EFAST	Extended Fourier Amplitude Sensitivity Test
EM	Electromagnetic spectrum
EVEOSD	Evaluation and Validation of EO-1 for Sustainable Development
EWT	Equivalent Water Thickness (leaf level) (g/cm^2)
EWT_{canopy}	Equivalent Water Thickness (canopy level) (g/cm^2)
FLAASH	Fast-Line-of-sight Atmospheric Analysis of Spectral Hypercubes
FMC	Fuel Moisture Content (% of dry matter)
FRT	Forest Reflectance and Transmittance model
FWHM	Full Width at Half Maximum
GSA	Global Sensitivity Analysis
GVMI	Global Vegetation Moisture Index
GVWD	Greater Victoria Watershed District
H	Tree Height (m)
LAI	Leaf Area Index (cm^2/cm^2)
LUT	Lookup Table
MLC	Maximum Likelihood Classifier
MNF	Minimum Noise Fraction
MSI	Moisture Stress Index
NDM	Needle Dry Mass (kg/tree)
NDVI	Normalized Difference Vegetation Index
NDWI	Normalized Difference Water Index
NIR	Near-Infrared
PCA	Principal Components Analysis
SD	Stand Density ($trees/m^2$)
SFSI	Shortwave Infrared Full Spectrum Imager
SLA	Specific Leaf Area (cm^2/g)
SLW	Specific Leaf Weight (g/cm^2)
SWIR	Short Wave Infrared
SWIR-1	1.0 - 1.8 nm
SWIR-2	1.8 - 2.5 nm
TASS	Tree and Stand Simulator
TIR	Thermal Infrared
WI	Water Index
6S	Second Simulation of the Satellite Signal in the Solar Spectrum model

List of Figures

List of Tables

Acknowledgements

Without the support and encouragement of many people, this work would never be possible. I would like to thank all those who helped, advised and encouraged me in the realization of this thesis.

Dr. David G. Goodenough deserves my deep gratitude for time, energy, suggestions, help, and encouragements he gave me, especially during difficult times. I have gained much experience from him and would like to thank him for all he has given. I am also grateful to David for providing me the invaluable opportunities of attending several IEEE conferences in remote sensing.

I would also like to thank Professor K. Olaf Niemann, Department of Geography, and Professor Wendy Myrvold, Department of Computer Science, University of Victoria who are also advisors of this thesis, for their teaching and advising. I'm grateful to Dr. Harold Zwick, Engineering Manager – Research and Development of MacDonald Dettwiler, for agreeing to serve as an external examiner.

Special thanks go to Andrew Dyk who shared his experience and provided me with the data to carry out my research at the Advanced Forest Technologies (AFT) lab, Pacific Forestry Centre (PFC), Natural Resources Canada, Canada. I would also like to thank Hao Chen at AFT for providing computing support with enduring patience and sharing research skills.

At AFT, I would like to thank all those who participated in the field campaigns and pre-processing of remote sensing images. Without their laborious task of collecting field data and processing remote sensing data, this work would never be possible either. At PFC, I am also grateful to Alex Song, A. Y. Omule and all other colleagues who supported and assisted me during my work.

Finally, I would like to thank my family for their understanding and support.

This research was funded by the Natural Sciences and Engineering Research Council (NSERC) of Canada.

Chapter 1

Introduction

1.1 Nature of the Moisture Problem

About 70 per cent of the Earth's land surface is covered with vegetation [1]. Virtually all types of vegetations are subject to wildfire [2]. The potential effects of wildfires include biodiversity, productivity, human health, and climate change. Fire events occur every year with different intensity and frequency. In North America, wildfires affect several million hectares with damage and control costs more than ten billion dollars per year [3]. In addition, studies in climate change have linked greenhouse gases to global warming. In Canada, from 1930 to present an average of 1.3×10^6 ha of forest is burned annually [4]. For Canada, which has 10 percent of the world's forests, and an obligation to meet its international commitments under the Kyoto Protocol, greenhouse gas emissions will become a growing concern over the next decade. As a result, there is increasing pressure to manage wildfires because CO_2 released from burned forests is a major source of greenhouse gas emissions [4, 5].

Operational fire management agencies face many challenges from predicting fire dangers to fire suppression in order to protect endangered communities, infrastructure, and commercially valuable forests. Information about vegetation status is particularly useful for evaluating and monitoring wildfire hazards. In the community of forest fire management, fuel moisture content (FMC), which is defined as the percentage of

moisture over dry matter, is considered as one of the key variables affecting fire ignition and propagation [6-9].

Several methods have been proposed to estimate FMC for wildfire management applications. These methods include field measurement, calculation of meteorological indices, and application of remote sensing techniques [10].

The most common method is field measurement. However, field measurements used to monitor forest biophysical parameters are expensive, difficult to repeat, and provide limited information because they only represent a small location, over a limited period of time. Lightning- and people-caused fires are the two main forms of wildfires. Studies showed that lightning-caused fires tend to destroy larger areas on average than people-caused fires because they can happen in more remote locations, where the fire detection and suppression may be delayed. This further limits the applicability of field sampling in estimating FMC [11, 12].

The second approach used by most operational fire danger rating systems is to estimate FMC based on meteorological data. This approach estimates FMC by taking into account meteorological variables that affect FMC, such as solar radiation, air temperature, air humidity, precipitation, and wind. Some authors also have attempted to obtain an indirect estimation of live FMC values from drought indices with the consideration of the medium- to long-term trends of atmospheric variation and soil water availability [13, 14]. However, this approach is not a direct estimation of FMC and not spatially

comprehensive because it only refers to the specific conditions where the weather stations are located [10].

Remote sensing with detailed and frequent observation of the earth's surface allows monitoring of the spatial and temporal variations of FMC [6, 8]. Therefore, in principle, remote sensing technology has the potential to overcome some of the above difficulties. It has the advantage of high spatial and spectral resolution, temporal consistency, mapping of large areas and quantifiable uncertainty [15]. In addition, remote sensing data is directly related to vegetation dynamic processes [16]. Compared with meteorological indices, remote sensing techniques have disadvantages related to temporal frequency, cloud coverage, and calibration. Section 2.5 reviews the methods for estimating FMC using remote sensing data.

1.2 Research Objectives

The research question for this thesis is whether with remote sensing data we can estimate fuel moisture content of forests. The fuel moisture content will be retrieved from remotely sensed data by inverting a canopy radiative transfer model. This is performed in two steps. First, ground measurements, stand dynamic models of Douglas-fir and ancillary data will be used to calibrate the model and generate a lookup table for fuel moisture content. Then, remote sensing hyperspectral data (such as AVIRIS and Hyperion) will be used to invert the model to estimate fuel moisture content. Accuracy will be assessed by comparing model results with field measurements and the water index

method. Finally, a software system will be developed for estimation of fuel moisture content of conifer forests.

1.3 Structure of the Dissertation

This dissertation is divided into seven chapters. Chapter 1 presents the nature of the problem and the research objectives. Chapter 2 introduces the background of remote sensing and vegetation water content, and also reviews the latest works on the sensitivity of reflectance to variations in vegetation at both leaf and canopy levels, and the methods for estimating FMC using remote sensing technique. Chapter 3 describes the study area, remotely sensed data, and ground measurements.

The methods being used in this study are presented in Chapter 4. It starts by describing the radiative transfer models for the leaf, canopy and atmosphere. After that, it discusses how to configure the model input parameters. Finally, it reviews the lookup table method for estimating forest foliage water content and assessment of its performance.

Chapter 5 documents the design and implementation of the computing system. Chapter 6 presents and discusses the results of sensitivity analysis, experiments with the water index method, the lookup table method, and the forest water mapping system. Finally, Chapter 7 concludes the research and discusses areas for future research and applications.

Chapter 2

Remote Sensing and Vegetation Water Content

This chapter presents the background information about remote sensing and vegetation water content. Section 2.1 evaluates the role of vegetation water content in forest ecosystems. Section 2.2 discusses the electromagnetic spectral regions that could provide information on vegetation and introduces hyperspectral remote sensing data. Section 2.3 provides the basic concepts behind vegetation water content at both leaf and canopy levels. Spectral response to variation in vegetation water content is discussed in section 2.4. Finally, section 2.5 reviews the methods for estimating vegetation water content.

2.1 Role of Vegetation Water Content in Forest Ecosystem

In a forest ecosystem, foliage water content is a critical factor for wildfire ignition and propagation and tree health. In general, the critical factors considered in a forest fire rating system include vegetation status (height, continuity, type, water content), terrain characteristics (slope, elevation), ignition sources (human-caused and lightning), and meteorological factors. Some of these factors do not need frequent updating, such as terrain characteristics, vegetation height and type. However, vegetation water content and meteorological factors require frequent updating for short-term risk assessment [17]. Meteorological danger indices may provide information on dead fuel moisture content. However, live fuel moisture content varies spatially and temporally due to the interaction

of plant physiology with soil moisture conditions. This variability is a significant challenge to fire management [18].

Figure 2.1 is an example of the Canadian forest fire danger rating systems. The Canadian Forest Fire Weather Index (FWI) System uses daily weather observations to estimate the moisture content of three different fuel classes and uses these to generate a set of relative indicators of potential rate of fire spread, fire intensity, and fuel consumption. The Canadian Forest Fire Occurrence Prediction (FOP) System predicts both lightning- and human-caused fires based partially on the fuel moisture levels as predicted through the FWI system. The Canadian Forest Fire Behavior Prediction (FBP) System systematically assesses fire behavior, such as fire Rate of Spread (ROS), Head Fire Intensity (HFI), Fuel Consumption (surface [SFC], crown [CFC] and total [TFC]), and a fire description code (surface, intermittent, or crown). FBP also needs foliar moisture content as one of the inputs. Among the four fuel characteristics: fuel type, fuel biomass, fuel moisture, and fuel condition, fuel moisture is potentially the most important factor that influences fire hazard [19]. High fuel moisture content implies that more heat is required to ignite a fuel and the fire propagation is slow, because part of the heat released by the fire is absorbed by the water from adjacent fuels [20]. In addition, fuel moisture content is a critical factor that converts a surface fire to a crown fire [21]. Several studies also reported the strong correlation between fire ignition likelihood and moisture content of live and dead fuels in grass, shrub, and forest fuels. The fresh foliage of Mediterranean shrubs becomes very flammable when the fuel moisture content drops below 75% [22]. The potential of crown

fire will increase in pine forests when the tree crown moisture content is below 100 per cent [23]. Fuel moisture content is a critical factor in any wildfire danger rating system.

Fuel moisture content is also one of the indicators of tree health. Healthy forests provide us with clean air and pure water. Forests also serve as habitats for wildlife and endangered species of plants and animals. Leaves are where the photosynthesis process occurs. Leaves use light as a catalyst, water from the roots and carbon dioxide absorbed from the air, to produce sugars. Water stress affects photosynthesis in two ways [24]. First, the closure of the stomata usually blocks access of the chloroplasts to the atmospheric supply of carbon dioxide. Second, low cellular water potential directly affects the structural integrity of the photosynthetic machinery. Therefore, water stress not only affects the forest ecosystem itself but also the carbon cycle in the earth system.

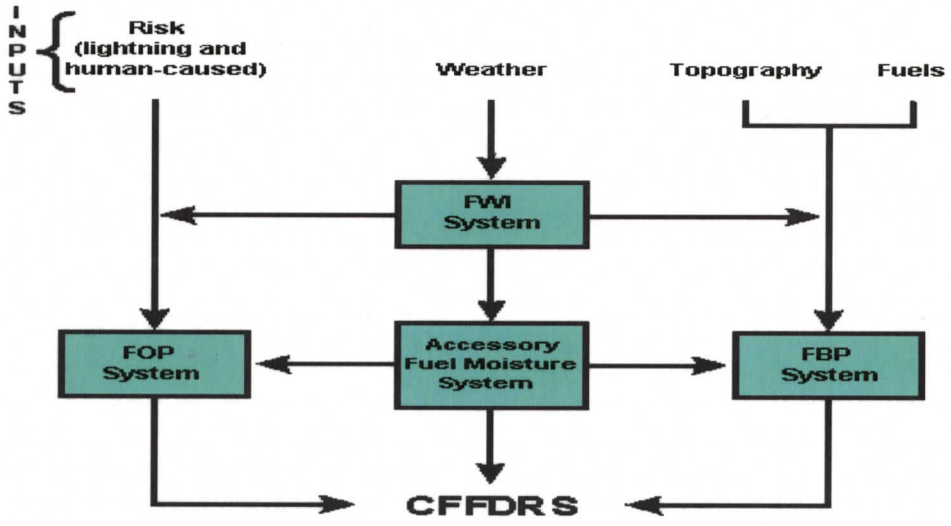

Figure 2.1 Canadian Forest Fire Danger Rating System (CFFDRS) [25].

2.2 Remote Sensing Background

2.2.1 The Electromagnetic Spectrum

All remote sensing systems rely on part of the electromagnetic (EM) spectrum to sense and record information about the earth's surface. Most systems rely on the sun to generate all the EM energy needed to image the earth's atmosphere and surfaces. These systems are called *passive sensors*. Other sensors generate their own energy, and are called *active sensors.* Active sensors transmit energy in a certain direction and record the portion reflected back by features within the signal path.

Five different wavelength regions in the EM spectrum could be used to monitor vegetation characteristics: Visible (VIS), Near Infrared (NIR), Short Wave Infrared (SWIR), Thermal Infrared (TIR), and Microwave. The EM energy from these regions can provide information on vegetation biophysical and biochemical features [1]:

- Visible (0.4 – 0.7 μm): Leaf pigments in typical green vegetation absorb light in the visible region. So this region is characterized by low reflectance and transmittance. Chlorophyll a and b are the most important leaf pigments that absorb blue and red light.

- NIR (0.7 – 1.0 μm): Due to scattering from the internal structure, a healthy vegetation leaf is generally characterized by high reflectance and transmittance, and relatively low absorptance. The leaf reflects 40-60 percent of the incident

NIR energy from the spongy mesophyll. The remaining 40-50 percent of the energy passes through the leaf and can be reflected by leaves below it, the process which is called leaf additive reflectance.

- SWIR (1.0 – 5.0 μm): In general, the more water content, the lower the leaf reflectance in this region. Conversely, as the leaf water content decreases, the reflectance will increase substantially. Leaf reflectance is a function of the total amount of water content and leaf thickness. The sensitivity of leaf reflectance to leaf water content is strongest in bands centered at 1450, 1940, and 2500 nm [26].

- TIR (5.0 – 16.0 μm): This region is quite different than the visible and reflected IR portions, as this energy is essentially the radiation that is emitted from the earth's surface in the form of heat. TIR data have been used to provide information about forest canopy structure, biomass, age, and physiological condition.

- Microwave (0.1 – 100 cm): Active microwave energy can penetrate the canopy to varying depths and interact with the canopy components. The backscattered energy depends on the nature of the energy sent and the structure and status of canopy. Therefore, microwave remote sensing can provide information about canopy water content, canopy structure, vegetation type, and biomass by component.

2.2.2 Hyperspectral Remote Sensing

Hyperspectral remote sensing, also known as imaging spectroscopy, is a relatively new technology that is currently being investigated by researchers and scientists with regard to the detection and identification of minerals, vegetation, and man-made materials. Imaging spectroscopy is based on the interaction and reflectance of photons with molecular structures of surface materials. Reflectance and emittance spectroscopy of natural surfaces are sensitive to specific chemical bonds in materials, whether solid, liquid or gas.

Hyperspectral imaging systems usually have hundreds of narrow contiguous bands of relatively narrow bandwidths (5-10 nm), while multispectral datasets are usually composed of 5-10 bands of relatively large bandwidths (70-400 nm). Most Hyperspectral imaging systems are able to collect images starting at about 400 nm. Typically these systems can measure energy up to 1100 nm (visible/near infrared, VNIR) or even 2500 nm (short-wave infrared, SWIR). The hyperspectral image cube provides a complete description of the spectral response characteristics of earth surface materials, and makes it possible to distinguish them even though they only have minor spectral differences, like crops and grasses. Examples of airborne hyperspectral imaging systems include the Advanced Solid-State Array Spectroradiometer (ASAS) [27], NASA's Airborne Visible/Infrared Imaging Spectrometer (AVIRIS) [28], the Canadian compact airborne spectrographic imager (CASI) [29], and the Shortwave Infrared Full Spectrum Imager

(SFSI) [30]. Figure 2.2 is a sample AVIRIS image of the Greater Victoria Watershed (GVWD).

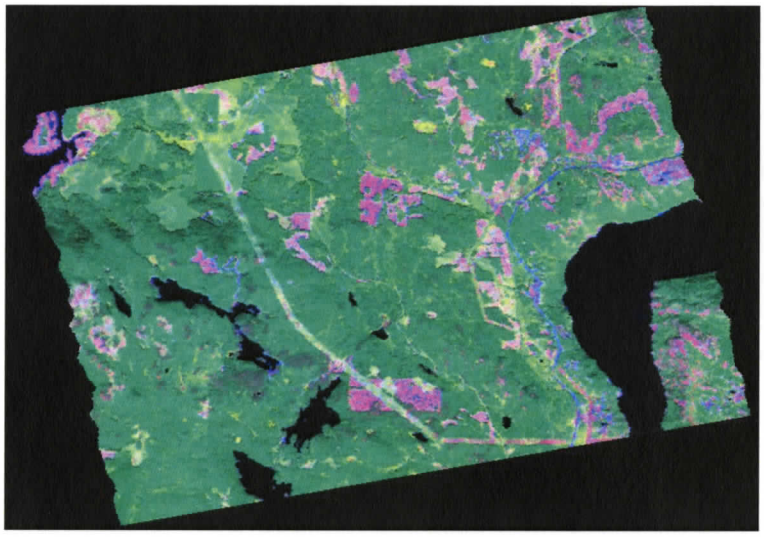

Figure 2.2 Sample AVIRIS image of GVWD acquired in August 2001 (RGB display of bands 1562, 759, and 615 nm; spatial resolution is 20 m; area shown is 141.66 km^2).

2.3 Vegetation Water Content: Leaf and Canopy Level

At the leaf level, vegetation water content is usually represented by the fuel moisture content (FMC) or equivalent water thickness (EWT). In the wild fire research community, FMC is one of the key input parameters to fire behaviour models since it is critical to fire ignition, burning efficiency, and fire propagation. FMC is a relative measure of vegetation water content obtained from measurements of leaf (needle) fresh and dry weight. FMC is computed as the amount of water content per unit of leaf dry weight expressed as a percentage [8]:

$$FMC\ (\%) = ((W_f - W_d)/W_d) \times 100 \qquad (2.3.1)$$

where W_f is leaf fresh weight and W_d is leaf dry weight.

EWT is expressed as the amount of leaf water content (in grams) per unit area of leaf (A) (in cm^2) [18]:

$$EWT\ (g/cm^2) = (W_f - W_d)/A \tag{2.3.2}$$

Another related leaf biophysical variable is specific leaf weight (SLW). SLW is the weight of dry matter per unit area of leaf:

$$SLW\ (g/cm^2) = W_d\ /A \tag{2.3.3}$$

SLW is the reciprocal of Specific leaf area (SLA, cm^2/g), which is used in tree physiology. In the remote sensing community, leaf dry matter content (DM, g/cm^2) is an alternative term to describe SLW.

Rearranging equations (2.2.1) - (2.2.3) shows that FMC is related to both EWT and SLW through

$$FMC\ (\%) = (EWT/SLW) \times 100 \tag{2.3.4}$$

Leaf Area Index (LAI) is defined as the one sided green leaf area per unit ground area in broadleaf canopies, or as the projected needle leaf area per unit ground area in needle

canopies. At the canopy level, leaf EWT (EWT_{leaf}) scales with leaf area index (LAI) and thus leads to canopy EWT (EWT_{canopy}):

$$EWT_{canopy} = EWT_{leaf} \times LAI \tag{2.3.5}$$

However, FMC does not scale with LAI. Therefore, canopies with the same FMC may have different LAIs and, consequently, very different EWT_{canopy}.

2.4 Spectral Response to Variation in Vegetation Water Content

For accurate estimation of vegetation water content (FMC or EWT either at leaf or canopy level), it is critical to use reflectance at the wavelength regions that are sensitive to the variable of interest and insensitive to other factors. Several research efforts using laboratory measurements and model simulations have analyzed the spectral response to change in vegetation water content. At the leaf level, Ceccato et al. [31] performed global sensitivity analysis (GSA) using an Extended Fourier Amplitude Sensitivity Test (EFAST) [32] and the PROSPECT model [33]. The EFAST allows the computation of the total contribution of each input factor to the output's variance. The total contribution includes the factor's main effect and all the interaction terms involving the factor. They found that, in the NIR region, reflectance variations are exclusively influenced by leaf internal structure and dry matter content; in the SWIR region, leaf reflectance is mainly affected by EWT and secondly by nitrogen (N) and dry matter content (C_m). Bowyer et al. [8] also used EFAST and PROSPECT to simulate the spectral response to change in

FMC (controlled by EWT and dry matter content) with chlorophyll content and the N parameter fixed. This study found that EWT affects leaf reflectance most strongly in the SWIR region with three peaks at 1420nm, 1940 nm and 2480 nm and also contributes significantly in the NIR region. The influence of dry matter content is most strong in the NIR region and less important in the SWIR region but has two pronounced peaks at 1725 nm and 2270 nm where the water absorption is weak. These works show that FMC is most important in the NIR and SWIR regions. The reflectance in these regions, especially in the peaks, should be used for estimating FMC at leaf level.

At the canopy level, in the work by Ceccato et al. [31], GSA was only performed for two wavelengths at 820 nm and 1600 nm. Bowyer et al. [8] coupled PROSPECT and GEOSAIL to conduct GSA at the canopy level. They simulated canopy reflectance for wavelengths between 400 nm and 2500 nm. They found that the importance of the EWT and dry matter content in explaining reflectance variability is more complicated. In the NIR region, dry matter content still dominates the variation of canopy reflectance. In the SWIR region, the reflectance variability is dominated by variation in fractional vegetation cover followed by LAI, solar zenith angle, and EWT. These results imply that it would be difficult to estimate FMC from canopy reflectance using water indices without consideration of vegetation coverage, LAI, and solar zenith angle.

2.5 Remote Sensing of Leaf Water Content

Studies in remote sensing of vegetation water content follow the patterns below:

(a) Estimation of leaf water content or canopy water content.

(b) Water content is expressed as FMC or EWT; for a single species, EWT could be converted to FMC by assuming constant SLW (EWT=FMC*SLW).

(c) Estimating water content from canopy reflectance or leaf reflectance.

(d) Research methods being used: regression techniques, water indices, or physical-based approaches.

(e) Type of Vegetation: grasslands, shrubs, or forests.

Section 2.5.1 presents common research approaches for retrieving vegetation water content from remotely sensed data. Research efforts to estimate vegetation water content (EWT or FMC) have employed remote sensing data either at the leaf level or canopy level. Although similar approaches have been applied in studies at both levels, estimation of leaf water content from canopy reflectance is further complicated by the fact that canopy structure and background (ground vegetation and soil) reflectance vary spatially, temporally, and with sensor view angle. Section 2.5.2 reviews the studies based on leaf reflectance. Section 2.5.3 summarizes the work based on canopy reflectance.

2.5.1 Research Methods

Vegetation water content estimation techniques can be divided into ratio techniques (indices), statistical methods and physical methods. The ratio techniques usually employ data in two or more wavebands [34-38]. Ratio techniques cannot take advantage of many different bands in hyperspectral data. Statistical methods include linear regression [39,

40] and artificial neural networks [41]. The statistical methods allow rapid processing of large amounts of remote sensing data. However, they require data-specific calibrations and thus are empirical. Physical methods estimate biophysical variables by inverting quasi-physical models [42, 43]. Physical methods depend on how well a leaf/canopy radiative transfer model can simulate the relationships between various leaf/canopy parameters and leaf/canopy reflectance. They are potentially more robust and accurate than empirical statistical methods for estimating biophysical parameters from remote sensing data because physical-based models can accurately relate vegetation optical and structural variables to images acquired from space [44].

2.5.2 Leaf Level

Although not the primary focus of this paper, the studies at leaf level provided a basis for a more detailed study at canopy level. Several studies focus on the estimation of leaf water content. Jacquemoud et al. [43] estimated leaf EWT by inversion of PROSPECT on leaf reflectance resulting in R^2 of 0.95 on fresh leaves and 0.54 for dry leaves. The hierarchical foreground/background analysis (HFBA) was used to successfully ($R^2 = 0.62$) extract leaf equivalent water thickness from leaf reflectance [45]. Ceccato et al. [17] have shown that a combination of SWIR and NIR is necessary to retrieve EWT at leaf level. In a recent study [46], leaf reflectance of different species were used to invert PROSPECT to estimate both dry matter (DM) and FMC. The simulation for EWT together with the one for DM did not predict FMC accurately (R^2=0.33). However, using the simulated DM from dry samples for each species improved greatly the results for the estimation of FMC (R^2=0.89).

2.5.3 Canopy Level

Research has shown that both EWT and FMC may be retrieved from reflectance at canopy level using similar techniques to those applied in leaf-level studies. Gao and Goetz [39] used AVIRIS imagery to derive equivalent water thickness (EWT) in vegetation using nonlinear and linear least squares spectral matching techniques, and achieved correlation coefficients of 0.78 between the estimated EWT and measured FMC. Jacquemoud et al. [42] extracted vegetation biophysical parameters by inversion of the SAIL model coupled with the PROSPECT model on Sugar Beet canopy reflectance data. The root mean square error (RMSE) of retrieved leaf EWT (cm) is less than 0.02. Serrano et al. [47] applied water indices to estimate canopy relative water content (RWC) of Chaparral vegetation from AVIRIS images. The best performance is obtained by using water index (WI) when only data from plots with green vegetation cover > 70% were considered ($R^2 = 0.88$). Ceccato et al. [48] developed a water index, called Global Vegetation Moisture Index (GVMI), and applied it to retrieve canopy EWT. The correlation between GVMI and canopy EWT is 0.76 for Shrub Steppe and Shrub Savannah, and 0.98 for Tree Savannah and Savannah Woodland. Chuvieco et al. [49] estimated FMC based on the ratio of NDVI and surface temperature, and the relative greenness (RGRE) using AVHRR bands for both grasslands and shrubs. A strong correlation ($R=0.683$, $p<0.001$) was found. In a modelling study by Riano et al. [46], a canopy is simulated as a stack of leaves. The estimation of FMC from the "canopy" reflectance using the simulation of EWT and DM gives $R^2=0.62$. It improves after calculating the average DM estimated for each species ($R^2=0.81$).

Chapter 3

Study Site and Data Sets

This section describes the study site, remote sensing data and field measurements.

3.1 Study Site

The study area, the Greater Victoria Watershed District (GVWD), is located on Vancouver Island, B.C. This 15 km by 23 km area is topographically diverse with a relief of about 600 meters and an average elevation of 400 m above mean sea level. Soils in the GVWD are classified as Orthic Dystric Brunisol. This watershed contains lakes and forests. The dominant forest type is Coastal Douglas-fir (Pseudostuga menziesii var. Menziesii). Secondary species include western hemlock (Tsuga heterophylla), western white pine (Pinus monticola), lodgepole pine (Pinus Contorta), red alder (Alnus Rubra), western redcedar (Thuja Plicata), and arbutus (Arbutus menziesii). The main ground vegetation is a mixture of salal (Gaultheria shallon) and Oregon grape (Mahonia nervosa) [40].

3.2 Ground Truth Measurements

In this study, we will use the field measurements that were collected as part of the Evaluation and Validation of EO-1 for Sustainable Development (EVEOSD) project at the Pacific Forestry Centre [50].This dataset contains foliar chemistry, field spectrometer

and GIS data. The samples include old growth, mature and immature Douglas-fir stands in a range of various slopes, aspects and elevations. During the field campaigns, a total of 1846 foliar samples of Douglas-fir and Salal were collected within an area of 200 square kilometers as shown in Figure 3.1 [50]. The samples were analyzed for organic constituents, chlorophyll a and b, total chlorophyll, moisture percentage, nitrogen percentage and inorganic components. Ancillary data include geographic position, site classification, dominant canopy, middle canopy, and ground cover.

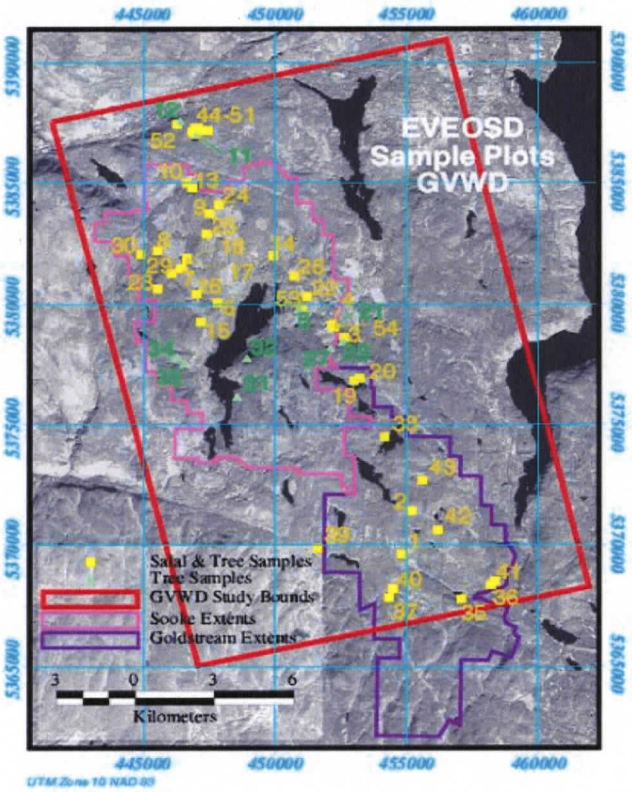

Figure 3.1 EVEOSD sample plots at GVWD (Yellow dots indicate sample plots for Salal and tree samples. Green dots indicate sample plots for trees only. The red box is the boundary of the GVWD test site. The image backdrop is the band 5 of Landsat 7 data and was acquired on September 10th, 2001).

3.3 Remote Sensing Data

The sensor named AVIRIS stands for Airborne Visible/Infrared Imaging Spectrometer, which was developed at the Jet Propulsion Laboratory (JPL), of NASA [28]. AVIRIS, usually flown on the ER-2 aircraft, measures the total upwelling spectral radiance in the solar-reflected spectrum from 400 to 2500 nm through 224 contiguous spectral channels at 10 nm intervals. Smooth and continuous spectra can be extracted from the AVIRIS images. The AVIRIS images have been widely used in a range of scientific research and applications, for example, atmosphere, geology, hydrology and forestry. The main AVIRIS parameters for the ER-2 platform are summarized in the following table.

Table 3.1 Main characteristics of AVIRIS.

Spatial Resolution	20 m
Field of View	30 degrees
Swath Width	10.6 km
Wavelength range	400 – 2500 nm
Pixels/Scan Line	614
Number of Spectral Bands	224
Sampling	10 nm
Spectral response (FWHM)	10 nm

The AVIRIS data used in this study were obtained through the EVEOSD campaign over the Greater Victoria Watershed District (GVWD) on August 10, 2001. Image pre-processing of AVIRIS was carried out through four steps:

(1). Atmospheric correction,

(2). Orthorectification and geometric correction,

(3). Force-fit to ground spectra, and

(4). Image Classification.

The atmospheric correction was performed using the **F**ast-**L**ine-of-sight **A**tmospheric **A**nalysis of **S**pectral **H**ypercubes (FLAASH) [51] in ENVI developed by Spectral Sciences, Inc.. FLAASH, using MODTRAN4 radiative transfer model, is a first-principles atmospheric correction-modeling tool for retrieving spectral reflectance from hyperspectral images. The noisy regions 1343 - 1432 nm and 1802 - 1949 nm were not processed. To execute FLAASH, several parameters are required, including scene center location, flight date and time, atmospheric model, and so on. The detailed information on the FLAASH parameters can be found in [51]. In this thesis, we set the following parameters for AVIRIS using FLAASH: continental atmospheric model, visibility of 30 km, water vapour and aerosol retrieval.

Geometric correction is undertaken to use georeferenced data and is achieved by establishing the relationship between the image coordinate system and the geographic coordinate system. During the EVEOSD campaign, Ground Control Points (GCPs) were collected for each AVIRIS scene. The geometric correction was completed using the

OrthoEngine software package developed by PCI Geomatics. Details of the geometric correction procedures were described in [52]. The geometric accuracies for the AVIRIS data were 4.2 m [53].

Force-fit [50] was performed to eliminate the remaining atmospheric effects (Figure 3.2). The force-fit is in fact a spectral calibration, which forces the AVIRIS spectra to fit the ASD ground spectra at the calibration locations. The force-fit function consists of a gain correction and an additive shift. Both corrections were applied for bands 6-31, 35-76, 78-96, 115-152, and 168-213 on a per-band basis. The omitted bands were either considered to be redundant or to lie in atmospheric absorption regions and were not processed.

The classification step was achieved first through Minimum Noise Fraction (MNF) transformation [54] and then by the Maximum Likelihood Classifier (MLC). Because hyperspectral imagery provides a continuous spectrum ranging from 400 to 2500 (in the case of AVIRIS) for a given pixel, it generates a large amount of data required for processing and analysis. The MNF transform is often used to reduce the dimensionality of the hyperspectral data. The MNF transform is a linear transformation which essentially consists of two cascaded Principal Components Analysis (PCA) transformations. The first transformation decorrelates and rescales the noise in the data. This step creates transformed data in which the noise has unit variance and no band to band correlations. The second transformation is a standard PCA of the noise-whitened data. The Maximum Likelihood Classifier (MLC) is based on Gaussian probability distribution functions for the probability estimation in the discriminate function. Among all supervised non-

contextual classification methods such as Minimum Distance, K-means, and K-Nearest Neighbor, MLC is considered to be the best in the sense of obtaining optimal recognition rates [55, 56]. The AVIRIS data were reduced to twelve MNF channels, which were used in the classification. Overall classification accuracies for the AVIRIS data were 90.5% for the truth data and 88.5% for the check data [53].

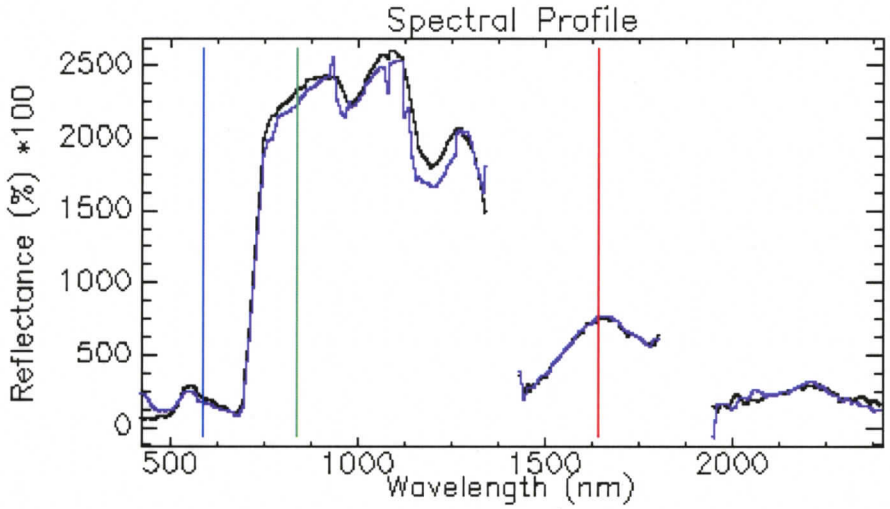

Figure 3.2 Spectral profile of Douglas-fir (The purple line is from the AVIRIS image before the force fit function was applied and the black line is from the image after applying the force fit function).

Chapter 4

Methodology

This chapter presents the methodology for retrieval of fuel moisture content from remote sensing data. First, Section 4.1 documents the radiative transfer models at leaf, canopy and atmospheric levels. The model, Forest Reflectance and Transmittance (FRT) model, used to simulate canopy reflectance, is introduced in Section 4.2. Section 4.3 details how the model input parameters were configured to generate lookup tables. Using the lookup tables and remote sensing data, Section 4.4 discusses how to retrieve the fuel moisture content from the remote sensing image. Finally, Section 4.5 shows how sensitivity analysis was performed and how accuracy assessment was conducted to evaluate the methodology.

4.1 Radiative Transfer Models

4.1.1 Leaf Level

Since leaves comprise the main surface of vegetation, the reflectance, absorption and transmittance properties of leaves are essential to the understanding of the radiative process within the vegetation canopy. Several leaf optical models have been proposed to describe the interaction of light with a vegetation leaf or needle. They are distinguished by the physical assumptions and by the complexity of the leaf being simulated. These models can be classified into four groups [57]:

- *Plate models:* A leaf is simulated as one or several absorbing plates. An example of this is the PROSPECT model developed by Jacquemoud and Baret [58], which is in widespread use in the remote sensing community.

- *N-flux models*: They consider the leaf as a slab of diffusing and absorbing material.

- *Stochastic and other radiative transfer models*: The leaf is partitioned into different tissues and its optical properties simulated by a Markov chain or a more classical approach directly based on the radiative transfer equation.

- *Ray tracing models:* They require a detailed description of the internal leaf structure and the optical constants of leaf material.

In this study, the PROSPECT2 [43] model was modified and coupled into FRT to compute leaf reflectance and transmittance. The input parameters for the leaf model include chlorophyll content, water content, and dry matter content.

4.1.2 Canopy Level

Over the last two decades, a great deal of effort has been placed on the modeling of vegetation canopy reflectance. The transfer of solar radiation within a vegetation canopy is a complex process. It is difficult to understand the complex relationships between canopy

properties and associated reflectance spectra without using a physical-based model. Although simple linear models, such as spectral indices, have been traditionally used to retrieve vegetation canopy variables from optical remote sensing data, recent studies have put more emphasis on physical-based models. Linear models cannot address the inherent nonlinear relationship between the electromagnetic radiation and vegetation canopy and thus sometimes perform poorly [59]. In addition, empirical linear models cannot deal with the variations in remote sensing data from different sensors with differing viewing angles and solar illumination conditions, spatial resolution or vegetation amount and canopy structure [60, 61]. Therefore, such linear methods have been mainly used to estimate total vegetation amount rather than the individual vegetation variables.

Physical-based models compute vegetation canopy reflectance from given canopy parameters (chlorophyll content, water content, soil spectrum, LAI, etc.) and a given sun-target-sensor geometry. They can be used to understand how reflected signals are formed and what are the important driving factors. Moreover, inversion of physical-based models can be performed to extract vegetation canopy variables. The currently existing canopy reflectance models can be broadly categorized into geometric models, turbid-medium models, hybrid models and ray tracing models.

Geometric models [61-63] use geometric optics and radiative transfer theory to compute the reflectance from a plant canopy as a function of various structural (e.g. tree shape, tree height) and spatial parameters (e.g. stand density). Different scenes are modeled as varying proportions of shadowed and illuminated tree crowns, and shadowed and

illuminated background. Such models are appropriate for and have been successfully used in sparse canopy situations.

In contrast, turbid medium models consider the plant canopy as a collection of absorbing and scattering particles, e.g., leaves and trunks, with given spectral properties which are distributed randomly in horizontal layers with specific orientations [64]. Turbid-medium models are more appropriate for applications in denser and horizontally uniform canopies [65].

The ray tracing model [66-68] is another class of physical-based models. A three dimensional canopy is simulated on a computer with the considerations of the arrangement and orientation of the vegetation. The Monte Carlo approach is commonly applied to study the scattering of light beams by plants. Although requiring intensive computing resources, these models allow a more realistic representation of the vegetation canopy [68].

Hybrid models apply the principles of both geometric and turbid medium models. In such models, vegetation canopy is simulated as a distribution of geometric objects which are composed of absorbing and scattering particles. The versatile hybrid models can be applied to both sparse and dense canopies. A hybrid forest reflectance model (FRT) by Kuusk and Nilson [69] was used for simulating canopy reflectance under various situations in this study. The choice of the FRT model is mainly based on availability and applicability for the forest species. In addition, it was also based on the fact that the FRT

model has undergone extensive validations and comparisons and been used in many applications [60, 70-76].

4.1.3 Atmospheric Level

The remote sensing from a spaceborne or airborne platform of the earth's surface is strongly affected by the presence of the atmosphere on the Sun-target-Sensor path. After the influence of the atmosphere, the solar radiation illuminates the earth's surface. Some of the incoming photons are absorbed by the surface and the remaining photons are reflected back to space. Therefore, the radiance measured by the sensor depends on the surface properties and is a useful signal. However, the signal is perturbed by the atmosphere through two processes, absorption and scattering. To properly interpret these measurements, it is necessary to remove the atmospheric effects as accurately as possible.

With the appearance of digital imagery of the earth, there have been considerable studies in correcting the images for the effects of the atmosphere. Several radiative transfer models have been developed that can be used for atmospheric correction algorithms. Among those, the two models most commonly used as atmospheric radiative transfer (RT) models are 6S [77] and MODTRAN [78]. These models simulate the physical behaviour of the photons on their Sun-target-Sensor path. The general procedure of a physically-based atmospheric correction algorithm is that by giving the at-sensor radiance of a pixel together with some other input parameters, the algorithm computes the

reflectance of the pixel. In this paper, the 6S model was coupled to the canopy reflectance model.

4.2 Forest Reflectance and Transmittance (FRT) Model

The FRT model incorporates the modified leaf optics models PROSPECT [43] and LIBERTY [79], atmosphere radiative transfer model 6S [77, 80], and the homogeneous two-layer canopy reflectance model MCRM2 [81].

Here we summarize the main characteristics of the FRT model [69]:

- FRT is a hybrid model that includes the properties of both geometrical and radiative transfer equation-based models.
- Several tree classes of different sizes and /or species are possible. Within each class, trees are considered identical.
- Tree crown envelopes are modeled as ellipsoids of rotation or cones in the upper and cylinders in the lower part. Leaves and branches are uniformly distributed in the crown and spherically oriented.
- FRT handles both single and multiple scattering of radiation within the canopy.
- The ground surface is assumed to be a homogeneous layer of vegetation.
- FRT works in the spectral range 400-2400 nm with the spectral resolution of 1 nm under any Sun and view directions.
- FRT can be used for both direct and inversion modeling. The inversion is performed

by minimizing a merit function.

The FRT model simulates a forest scene as four components: sunlit tree crowns, sunlit ground vegetation, shaded crowns, and shaded ground vegetation. The directional spectral reflectance of a forest stand is calculated as follows:

$$\rho(r_1, r_2) = \frac{I_\lambda}{Q_\lambda} \rho_I(r_1, r_2) + \rho_D(r_1, r_2) \tag{4.2.1}$$

where:

r_1 = unit vector in the Sun direction,

r_2 = unit vector in the view direction,

$\rho(r_1,r_2)$ = directional spectral reflectance in direction r_2 with illumination in r_1 direction,

I_λ = direct down-welling flux (W/m^2),

D_λ = diffuse down-welling flux (W/m^2),

$Q_\lambda = I_\lambda + D_\lambda$, total down-welling flux (W/m^2),

$\rho_I(r_1,r_2)$ = single scattering reflectance factor, and

$\rho_D(r_1,r_2)$ = diffuse reflectance factor.

The single scattering reflectance factor $\rho_I(r_1,r_2)$ accounts for the single scattering from the tree crown $\rho_{I\_CR}(r_1,r_2)$ and single scattering from ground vegetation and soil $\rho_{I\_GR}(r_1,r_2)$,

$$\rho_I(r_1,r_2) = \rho_{I\_CR}(r_1,r_2) + \rho_{I\_GR}(r_1,r_2) \tag{4.2.2}$$

Single scattering from tree crown is part of the reflectance caused by photons scattered once on a tree crown element. It is calculated separately for all tree classes as follows (Figure 4.1):

$$\rho_{I\_CR}(r_1, r_2) = \sum_{j=1}^{m} \rho_{I\_CRj} \tag{4.2.3}$$

$$\rho_{I\_CRj} = \lambda_j c_j \iiint_{V_j} u_j \Gamma_j(r_1, r_2) p_{00j}(x, y, z; r_1, r_2) dx dy dz / \cos\theta_1 \tag{4.2.4}$$

where:

m = the number of tree classes,

λ_j = the number of trees of the *j* th class per unit ground area, i.e., stem density,

The x-, y-, and z-coordinates define a point within the tree crown,

$u_j = u_j(x,y,z)$, the foliage area volume density within a tree crown,

$\Gamma_j(r_1,r_2)$ = the scattering phase function of the canopy medium,

$p_{00j}(x,y,z; r_1,r_2)$ = the bidirectional gap probability of two simultaneous free lines-of-sight in directions r_1 and r_2 from the point (x,y,z) within a crown of the *j* th tree class,

c_j = the coefficient accounting for the deviations in the tree distribution pattern from the Poisson distribution,

V_j = the spatial region corresponding to the crown envelope, and

θ_1= the Sun zenith angle.

The bidirectional gap probability p_{00j} is defined as a product of two independent probabilities:

$$p_{00j} = p_1 p_2 \quad (4.2.5)$$

where p_1 is the within-crown level bidirectional gap probability and p_2 is that of the between-crown level.

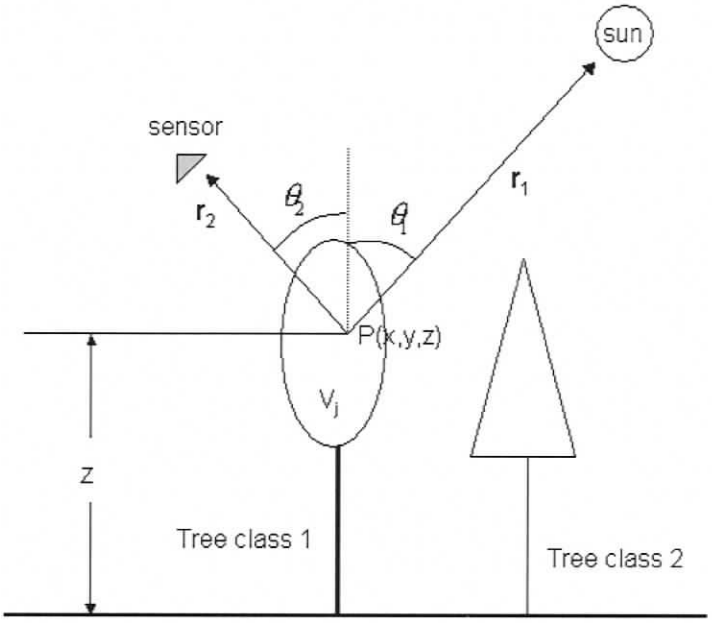

Figure 4.1 Single scattering from tree crowns of multiple tree classes (θ_1 is the Sun zenith angle and θ_2 is the view/sensor zenith angle. V_j is the crown envelope of the j^{th} tree class, x-, y-, and z-coordinates define a point P within the crown).

Single scattering from ground vegetation and soil is the product of the reflectance properties of the ground surface calculated by the MCRM2 model and the bi-directional gap probability. It is calculated by:

$$\rho_{I\_GR} = \rho_{GR}(r_1, r_2)\, p(r_1, r_2) \quad (4.2.6)$$

where:

$\rho_{GR}(r_1,r_2)$ = reflectance of ground surface in directions r_1, r_2, and

$p(r_1,r_2)$ = the bi-directional gap probability at ground level in directions r_1, r_2.

Diffuse reflectance factor $\rho_D(r_1,r_2)$ accounts for the multiple scattering from tree crowns and ground vegetation, and the diffuse radiance of scattered/reflected sky radiation D_λ,

$$\rho_D(r_1,r_2) = \rho_{D\_CR}(r_1,r_2) + \rho_{D\_GR}(r_1,r_2) \quad (4.2.7)$$

Multiple scattering is the reflection caused by photons scattered more than once by q tree crown, ground vegetation or soil. Diffuse fluxes of multiple scattering and diffuse sky radiation are treated as four flux approximations as in the SAIL model [82] and in the MCRM2 model [81]. For the differential equations that define the four fluxes and how the equations are solved, see FRT User Guide [83] for further reading.

4.3 Configuration of Model Input Parameters

The input parameters of the FRT model have to be configured accurately in order to have a realistic representation of the forest canopy. An example of an input file for FRT can be seen in Appendix A.1. This section describes the most important parameters of FRT (4.3.1) and shows how we configured the model input parameters (4.3.2).

4.3.1 Input Parameters of FRT

To run the FRT model, five sets of input parameters are needed:

(1) stand structural parameters,

(2) leaf biochemical parameters,

(3) parameters for ground vegetation and soil ,

(4) atmospheric parameters, and

(5) view geometry parameters.

Stand structural parameters represent the geometric properties of a forest scene in three dimensions. How these parameters are set affects the computation of canopy closure, leaf area index (LAI), shaded area of canopy and ground surface, etc. These variables include stand density (SD, trees/m^2), tree height (H, m), crown shape, crown length (m), crown radius (m), diameter at breast height (DBH, cm), total needle dry mass (NDM, kg/tree), specific leaf weight (SLW, g/m^2), ratio of branch area index (BAI) and leaf area index (LAI).

Leaf biochemical parameters for the PROSPECT model include chlorophyll content (% of SLW), water content (% of SLW), and dry matter content (% of SLW). Parameters for ground vegetation include LAI of ground vegetation, biochemical content (chlorophyll, water, dry matter, and brown pigment) of leaves, two leaf angle distribution parameters, and specific leaf weight (SLW).

4.3.2 Configuration of Input Parameters

Since our purpose is to estimate leaf water content for closed canopy conditions, the most important variables are the first two sets of parameters. Three approaches were used to set the model input parameters. The first approach was to use the mean values obtained from field measurements stored in the EVEOSD database. The second approach was to use values recommended in the literature. The third approach was to derive structural parameters based on stand dynamic models for Douglas-fir forests derived from local measurements. The other parameters except view geometry were set to the default values of FRT model. The Sun zenith angle was computed based on the acquisition time of the AVIRIS image. The view nadir angle was set to zero since the AVIRIS sensor is a nadir-viewing device [28] with a scan angle of 30 °. The FRT model does not include BRDF effects.

For each tree height class, the stand density was derived from the results modeled by the Tree and Stand Simulator (TASS) model [84, 85]. DBH (cm) was computed from tree height H (m) by the following regression model derived from field measurements on natural Douglas-fir:

$$DBH = C_1H^2 + C_2H + C_3 \qquad (4.3.1)$$

where $C_1 = 0.0266$, $C_2 = 0.546$, and $C_3 = -0.8565$.

Then, most of the other structural parameters were estimated via regressions on tree height (H, m) and diameter at breast height (DBH, cm).

Crown length (CL, m) was calculated by the regression model derived from local measurements of Douglas-fir:

$$CL = C_4 + C_5H + C_6DBH \tag{4.3.2}$$

where C_4 = -5.663, C_5 = 0.683, and C_6 = -0.0144. Crown radius (CR, m) was determined via the regression used by Nilson [86] for pine:

$$CR = (C_7\,DBH + C_8\,DBH/H)/2 \tag{4.3.3}$$

where C_7 = 0.1060 and C_8 = 0.6150. Total needle dry mass (NDM, kg/tree) was computed by the following biomass equation for foliage:

$$ln(NDM) = C_9 + C_{10} ln(DBH) \tag{4.3.4}$$

where C_9 = -2.8462 and C_{10} = 1.7009 (*ln* is natural logarithm).

Specific leaf weight (SLW) for Douglas-fir was set to 291.5 g/m^2 based on the specific leaf area value of 34.3 cm/g^2 taken from the literature[87]. The BAI to LAI ratio was set to 0.18 [86]. Chlorophyll content was set to 0.68 (% of SLW) which was the average

value of chlorophyll content computed from the chemistry measurements stored in the EVEOSD database. Tree crowns were modeled as cones in the upper part and cylinders in the lower part. Table 4.1 lists the values of the input parameters for the 6S model [83].

Table 4.1 Values of the major input parameters for the 6S model.

Parameter Name	Meaning	Unit	Values
iaer	Aerosol model -1 for BRDF, no sky radiation 0 no aerosol 1 for continental model 2 for maritime model 3 for urban model		2
c(i)	Volume percentage of each component c(i) in the atmosphere c(1) for fraction of dust-like component c(2) for water-soluble component c(3) for oceanic component c(4) for soot component		 0.70 0.29 0. 0.01
v	visibility	km	30
tau_aer (550nm)	Optical thickness at 550 nm		0.060
Sun zenith		degrees	33.4
View nadir angle		degrees	0

In the forest reflectance simulation, the trees within a plot were assumed to be identical. The procedure for generating the LUT table by the FRT model is illustrated in Figure 4.2. First, fixed parameters (e.g. LAI, DBH) are determined by the EVEOSD chemical database and other available ancillary information. The free parameters including FMC change within a certain range. Then, each value of free parameters, together with the fixed parameters, will feed into the FRT model to compute the reflectance corresponding to that water content. The simulated reflectance was integrated into AVIRIS bands using a Gaussian function and the bandwidth (FWHM) of each AVIRIS band. Finally, a lookup

table is generated and stored. Each entry of the table is a pair of the water content and the reflectance.

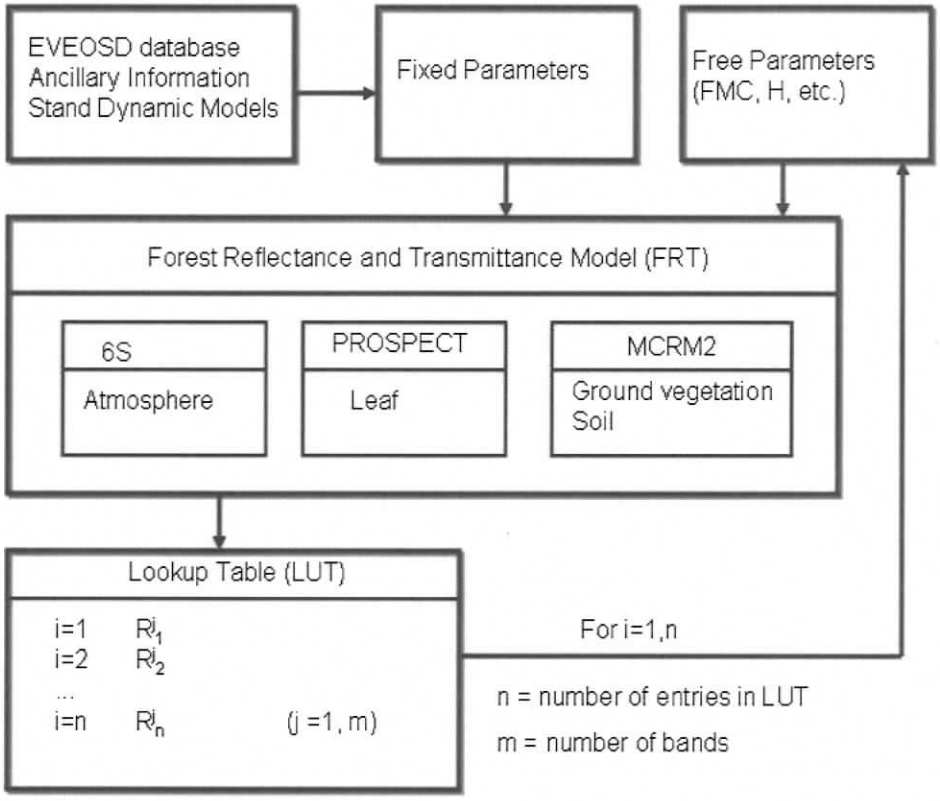

Figure 4.2 Flow chart for generating lookup tables using the FRT model (R_n^j is the simulated canopy reflectance for FMC(n) at wavelength j).

4.4 Model Inversion: Lookup Table Method

In order to extract the forest biophysical parameters using the canopy reflectance model, it is necessary to invert the model. However, the inverse problem is by nature an ill-posed problem because the solution is not unique and the measurement and model uncertainties may induce large variations in the solution [88].

Several approaches have been used to handle the ill-posed problems. Jacquemoud et al. [42] fixed some of the six canopy variables (chlorophyll a+b concentration, water depth, leaf area index, leaf mesophyll structure, mean leaf inclination angle, and hot-spot size parameter) and then estimated the rest as free variables. Inclusion of *a priori* information was attempted by Combal et al. [88] in the retrieval of canopy biophysical variables, and three different sources of *a priori* information were suggested. The first class of *a priori* information were ancillary data measured on site or products provided by another sensor, e.g., leaf water content (C_w) estimated with radar or subpixel heterogeneity derived from a higher resolution image. The second class referred to knowledge of the type of canopy architecture. The last class corresponded to the knowledge of typical distributions of canopy biophysical variables which strongly depend on the canopy type and development stage. The implementation of using priori information differs in each inversion algorithm. Kurz et al. [89] proposed a scheme to include ground control information in the inversion process by using a simple empirical model to fit simulated results to measurements. This study, as was presented in section 4.3 for TASS, tried to use the knowledge of the canopy structure of Douglas-fir.

Because of the complexity of canopy reflectance models, it is usually impossible to invert the model analytically and thus numerical methods are required. As an illustration, consider a model **M** with $\boldsymbol{p}$ unknown parameters, the vector **X** of explicative variables, and the vector **R** of observed variables. **X** is related to **R** through the relation:

$$\mathbf{R} = \mathbf{M}(\mathbf{U}, \mathbf{X}) + \boldsymbol{e} \qquad (4.4.1)$$

where **U** is the vector of the p unknown parameters. The inversion procedure refers to estimating **U** given **R**.

Two methods to solve the inverse problem are the optimization method and the lookup table method (LUT) [90]. The major disadvantage of optimization is that it is computationally intensive and, therefore, not appropriate for applications on a per pixel basis at regional or global scales.

One of the solutions to overcoming the high computational demand of the optimization method is the Lookup Table method (LUT). The LUT approach requires construction of a table of pre-calculated spectral directional reflectance data as a function of the key canopy biophysical variables [91]. The inversion process is reduced to searching the resulting tables for the reflectance values that most closely fit the measurements and then retrieval of the corresponding canopy biophysical variables. In the LUT method, many variables have to be fixed and the dimensions of the table have to be large enough to achieve a high degree of accuracy [90]. To select the solution of the inversion problem, a simple root mean square error (RMSE) is used as searching criteria:

$$\mathrm{RMSE} = \sqrt{\frac{\sum_{i=1}^{n} (R_i - R_{i,LUT})^2}{n}} \qquad (4.4.2)$$

where R_i is the measured reflectance for wavelength I and $R_{i,LUT}$ is the reflectance simulated by the FRT model and stored in the LUT. Interpolation may be required during the searching process because the intervals cannot be infinitely small. In this study, we used the LUT method to retrieve forest water content.

Figure 4.3 shows the flow chart, which is modified from that by Myneni et al. [92], illustrating the inversion procedures using the LUT method for estimating the canopy water content. The FMC value is obtained searching from the whole lookup table with measured reflectance as the search key. A merit function is computed, which compares the measured reflectance of a pixel with the modeled reflectance. If the merit function satisfies the threshold, the estimated water content will be assigned to this pixel and written to disk. Otherwise, the modeled reflectance of another entry in the LUT will be used for the next iteration. If none of the modeled reflectances satisfied the threshold, the one with the smallest merit function would be used for retrieving water content.

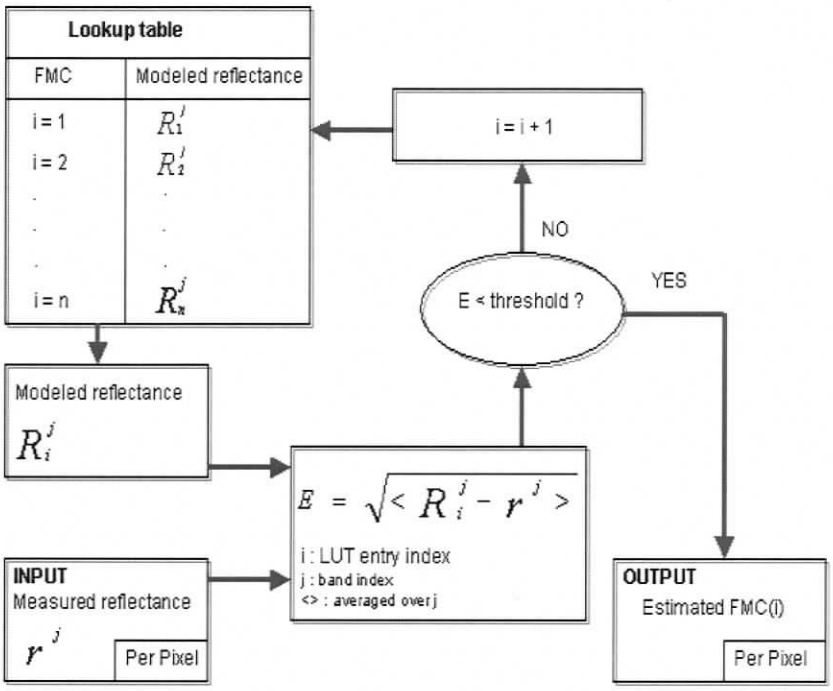

Figure 4.3 Inversion procedures for estimating FMC of forest (R is the modeled reflectance stored in LUT and r is the reflectance measured by satellite or airborne sensors).

4.5 Sensitivity Analysis and Accuracy assessment

The objective of sensitivity analysis is to select the wavelengths that are sensitive to FMC and differentiate the contribution from other factors. At canopy level, a simple sensitivity analysis was performed by changing a parameter of interest and fixing all other parameters. It allows the analysis of the response of canopy reflectance to the variations in that parameter. Chapter 6 presents the results of the sensitivity analyses.

To evaluate the performance of the proposed method, two types of accuracy assessment were conducted. First, we compared the estimated FMC with field measured FMC. Secondly, we compared the accuracy of the model inversion method (FRT) with that of the water index method.

Chapter 5

Computing System (FMAS) Design and Development

A new computing system, fuel moisture content (**F**MC) **ma**pping **s**ystem (**FMAS**), was designed and implemented to retrieve fuel moisture content of Douglas-fir from hyperspectral remote sensing images. This chapter documents the design and implementation of the system. The programs for each module of the system are listed in the appendix sections (A.2 – A.4).

5.1 Computing System (FMAS) Design

The expected users of this computing system are researchers who are interested in retrieval of forest water content by using physical-based approaches. During implementation of the computing system, we have the following requirements to consider:

- Ease of use: small training time; help frames and documents.
- Easy to modify.
- Reasonable Processing Speed.

The computing system consists of three software modules: reflectance simulation module, LUT generation module, and FMC estimation module (Figure 5.1). The main functionality, input, and output of each module are described as follows:

Reflectance Simulation Module

- *Functionality*: generates forest scenes with different biochemical and biophysical conditions and simulates canopy reflectance for each scene.
- *Input*: a basic input file that describes biochemical and biophysical characteristics of a forest scene.
- *Output*: canopy reflectance at 400 nm to 2400 nm with 1 nm interval for a forest scene.

LUT Generation Module

- *Functionality*: integrates simulated canopy reflectance into AVIRIS-equivalent reflectance and generates a lookup table with one entry for each realization.
- *Input*: canopy reflectance at 400 nm to 2400 nm with 1 nm interval simulated by FRT model.
- *Output*: a lookup table that contains values of free parameters and simulated AVIRIS-equivalent reflectance.

FMC Estimation Module

- *Function*: retrieves FMC for each Douglas-fir dominant pixel in a hyperspectral image.
- *Input*: a lookup table and a pre-processed hyperspectral image.
- *Output*: a FMC distribution map for Douglas-fir dominant plots.

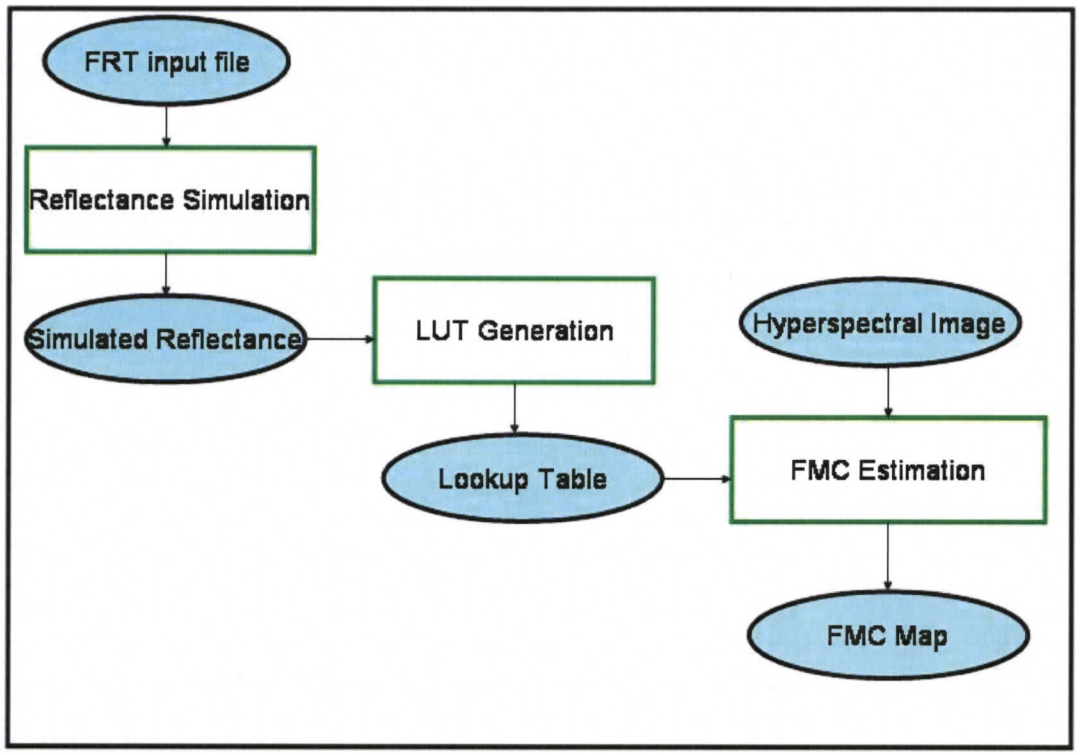

Figure 5.1 Components of the Fuel Moisture Content Mapping System (**FMAS**).

5.2 Programming Languages

The computing system **FMAS** was implemented by integrating the FRT model coded in FORTRAN-77 and three new software modules. The system was developed under a UNIX and PC environment. Software packages Perl, Matlab (**Mat**rix **lab**oratory), the Interactive Data Language (IDL) and the Environment for Visualizing Images (ENVI) were used.

Perl is an acronym for "**P**ractical **E**xtraction and **R**eport **L**anguage". Perl is an interpreted programming language known for its power and flexibility. It combines the familiar syntax of C, C++, sed, awk, grep, sh, and csh into a tool that that is more powerful than the separate pieces used together. Because of its powerful pattern matching capability, PERL was used to process the basic input file of the FRT model and produce different input files for each forest scene.

Matlab is an interactive program for numerical computation and data visualization. Matlab is especially designed for matrix computations: solving systems of linear equations, computing eigenvalues and eigenvectors, factoring matrices, and so forth. In addition, it has a variety of graphical capabilities, and can be extended through programs written in its own programming language.

IDL, developed by Research Systems, is a complete computing environment for the interactive analysis and visualization of data. IDL integrates a powerful, array-oriented language with numerous mathematical analysis and graphical display techniques.

ENVI is an image processing that provides comprehensive analysis of satellite and aircraft remote sensing data. ENVI is written entirely in IDL. ENVI combines file- and band-based approach to image processing. It allows the user to work with entire image files, individual bands, or both. ENVI also includes tools to extract spectra and analyze high spectral resolution images. ENVI handles all of pre-processing, post-processing steps such as input, output, display, analysis, and file management after implementing a user function. By employing ENVI's user function capability, programs written in IDL

can be integrated into the ENVI menus (interface). ENVI provides a library of functions and programming tools for user functions to handle input, output, plotting (including map composition), reports, and file management. Thus, ENVI was chosen as the implementation environment for the fuel moisture content (FMC) estimation module.

5.3 FMAS Implementation

The new computing system **FMAS** consists of more than 11,000 lines of code. Efforts were put at both understanding the canopy reflectance model FRT and programming the three new modules. The reflectance simulation module was implemented in PERL. Appendix A.2 lists the program. This program was used to simulate canopy reflectance of forest realizations with tree height (H), FMC, and needle dry mass (NDM, kg/tree) as independent variables. Needle dry mass is the mass of the needles in tree excluding water content. The program includes three loops each for a free parameter. Five tree height classes and their corresponding stem densities (SD) were used. Within an iteration of tree height, DBH was computed from SD and H. Then cylinder length, crown radius and length were calculated from H and DBH. The range of needle dry mass also depends on tree height. FMC changes from 80% to 220%. The FRT model was called to simulate reflectance for each combination of the three free parameters.

The LUT generation module was implemented using Matlab. This program is relatively short and could be converted to other languages, like IDL and FORTRAN. Appendix A.4

lists the program. The following procedure was used to compute the AVIRIS-equivalent reflectance:

1. For each forest scene
2. Extract free parameters
3. For each AVIRIS-band
4. Compute parameters for Gaussian function using the full width at half maximum (FWHM) and the center wavelength of this band
5. Find the band in the simulated reflectance stored in LUT
6. Integrate over the simulated reflectance using Gaussian function
7. END
8. END

The FMC estimation module was developed in ENVI environment and coded in IDL. The main steps of this module (A.4) were summarized as following:

1. Open an image and its classification mask through a GUI window
2. Load the LUT
3. For each Douglas-fir dominant pixel p_i
4. Extract measured reflectance at 903, 1192, and 1650 nm
5. If p_i is the first working pixel
6. Search the whole LUT to find the best matching entry e_j

   Else
7. Using its neighbour pixel LUT entry $e_{neighbour}$ as reference, search the LUT locally to find the best matching entry e_j
8. $e_{neighbour} = e_j$
9. p_i (FMC) = e_j (FMC)

The following functions of ENVI/IDL were used in the implementation of the FMC estimation module:

- ENVI_SELECT: A function used for file selection and spatial and spectral subsetting.
- ENVI_FILE_QUERY: A function used to get the filename and X and Y starting pixel.
- ENVI_GET_DATA: A function that returns any image band that is already opened (i.e., it appears in the Available Bands List of ENVI).
- ENVI_REPORT_INIT and ENVI_REPORT_INC: Functions for processing status reports.

A graphical user interface (GUI) (Figure 5.2) will pop up when you run this module, which makes it easy to use. In this interface you open the hyperspectral image, select the mask, and then run the program. Appendix A.5 shows how to run this module step by step. Figure 5.3 is a sample fuel moisture content (FMC) map generated by the FMAS system. The AVIRIS image was obtained on August 10th, 2001 and pre-processed as described in section 3.3. The accuracy of the estimated FMC will be discussed in the next chapter.

The processing speed depends on the dimensions of the lookup table. It took about 3 hours to generate a 3-D LUT on a computer with 3 GHZ CPU. To retrieve FMC from a 735×1000 AVIRIS image, FMAS took about 9 hours. Parallel computing can be used to

solve this problem. All the processors on a parallel architecture, for example a Linux cluster, can be used to run the same code on different parts of the image simultaneously. Since the algorithm only involves simple pixel operations, the image can be divided into a number of pieces. These pieces of data are distributed equally among all the processors for processing [93]. A linear speed up as a function of the number of processors can be achieved.

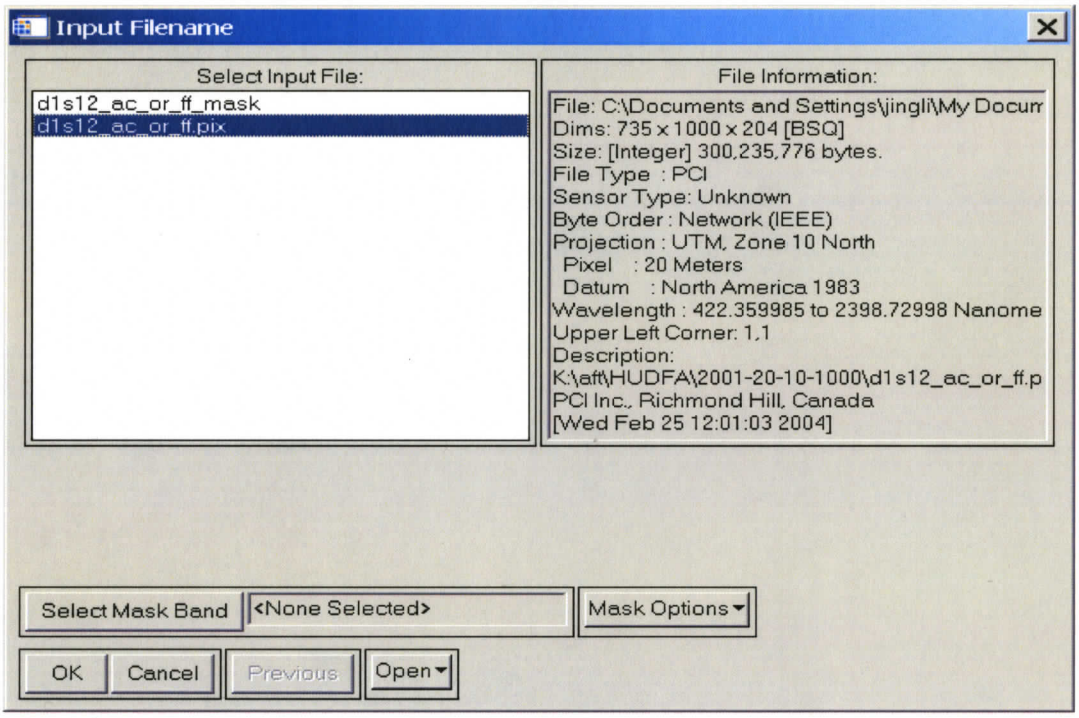

Figure 5.2 The GUI for FMC Estimation Module.

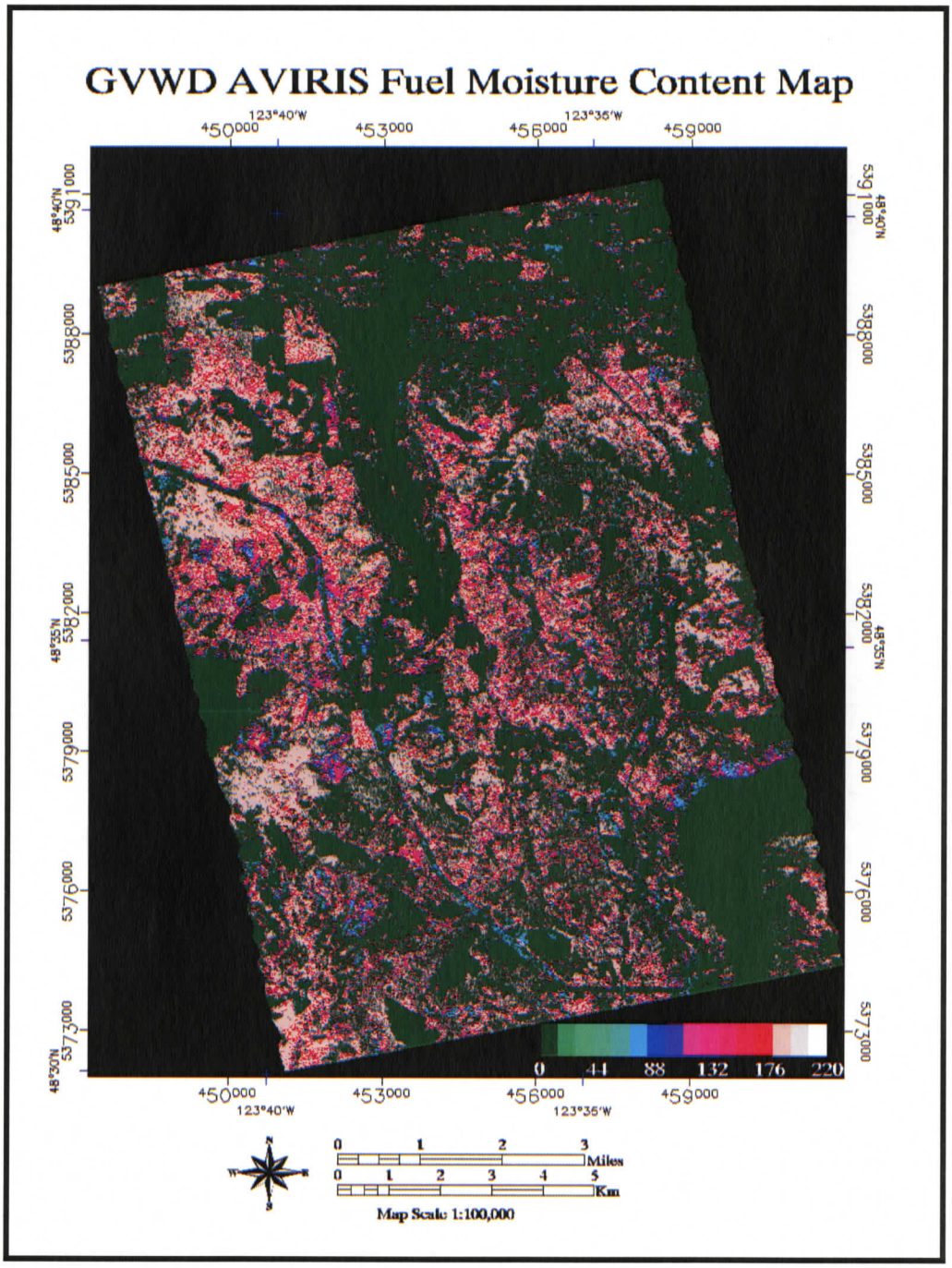

Figure 5.3 FMC map of Douglas-fir dominant pixels at GVWD (August 10th, 2001; Dark green areas are either not Douglas-fir dominant or are non-vegetated. FMC accuracies were $R^2 = 0.32$ for pure Douglas-fir plots with tree height larger than 28.4 m; $R^2 = 0.74$ for Douglas-fir dominant plots with tree height larger than 37.4 m).

Chapter 6

Results

This chapter presents and discusses the results of sensitivity analysis, the water index method, and the lookup table method.

6.1 Sensitivity Analysis

6.1.1 Fuel Moisture Content

Figure 6.1.1(a) shows the canopy reflectance values simulated by FRT with FMC changing from 80% to 240% and other parameters fixed (LAI =6.86). Since SLW is fixed, the variations in FMC are totally due to the changes in leaf EWT. As FMC increases from 80% to 240%, it has no impact on the visible region; but the canopy reflectance values increase in both NIR and SWIR region. Figure 6.1.1(b) shows the variations of canopy reflectance when FMC changes from 80% to 240%. The variation is defined as $(R_{FMC=80\%} - R_{FMC=240\%})/ R_{FMC=80\%}$. It shows that in the NIR region the variations of canopy reflectance are less than 15% with a peak at water absorption wavelength around 970 nm, and the variations are strong over the whole SWIR region with three peaks around 1200 nm, 1400 nm and 1850 nm. It suggests that 970, 1200, 1400, 1850 nm are the best candidate wavelengths for retrieving FMC.

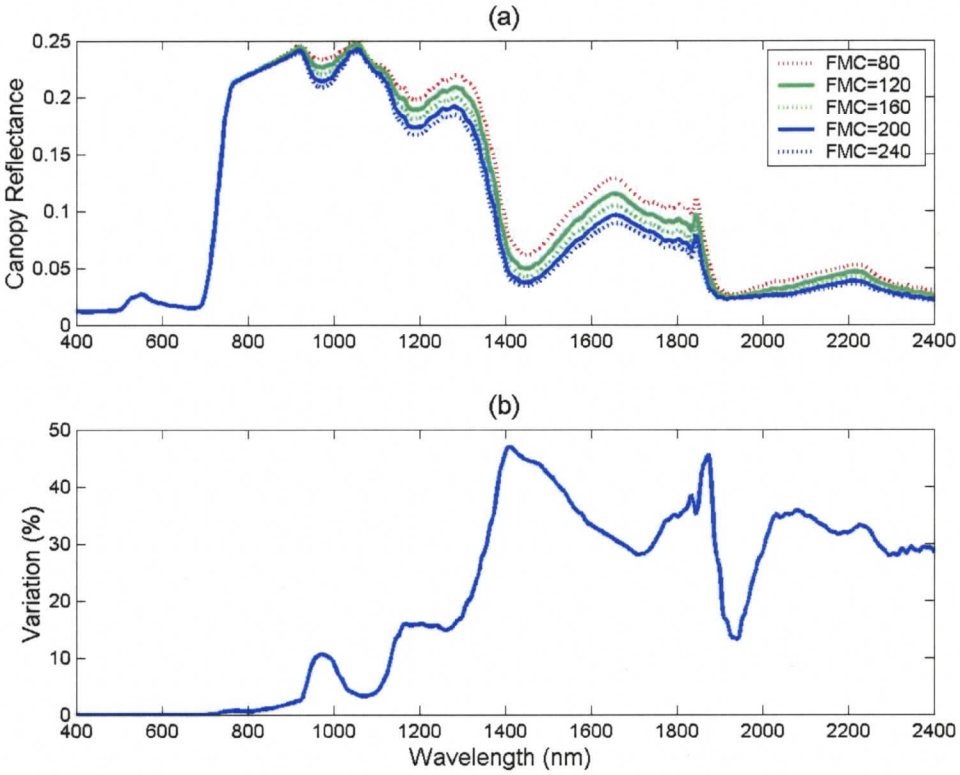

Figure 6.1.1 (a) Canopy reflectance simulated by FRT model with FMC of 80%, 120%, 160%, 200%, and 240%; (b) Variations (%) of simulated canopy reflectance with FMC changing from 80% to 240%.

6.1.2 Leaf Area Index (LAI)

LAI scales with water content from leaf level to canopy level. Figure 6.1.2 shows that LAI has a similar influence on canopy reflectance as FMC in the SWIR region. The variation is defined as $(R_{LAI=2.74} - R_{LAI=6.86})/ R_{LAI=2.74}$. The sensitivity of canopy reflectance to LAI is weak in NIR region even at 970 nm. In addition, LAI also affects the visible region.

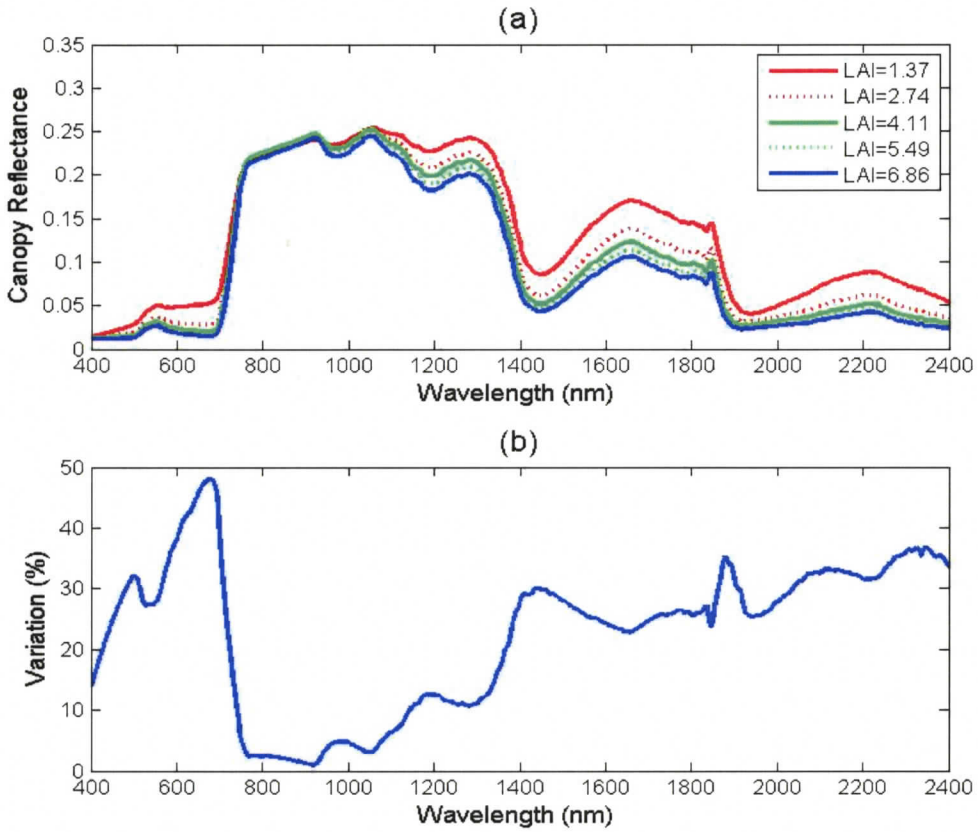

Figure 6.1.2 (a) Canopy reflectance simulated by FRT model with LAI of 1.37, 2.72, 4.11, 5.49, and 6.86; (b) Variations (%) of simulated canopy reflectance with LAI changing from 2.74 to 6.86.

6.1.3 Canopy Closure

In this experiment, the variation is defined as $(R_{CC=58\%} - R_{CC=93\%})/ R_{CC=58\%}$. Figure 6.1.3 shows that canopy closure has a very strong influence on canopy reflectance in the NIR and SWIR-1 region and weak in other parts. When canopy closure increases from 58% to 93%, canopy reflectance increases by almost 40 % in the NIR region.

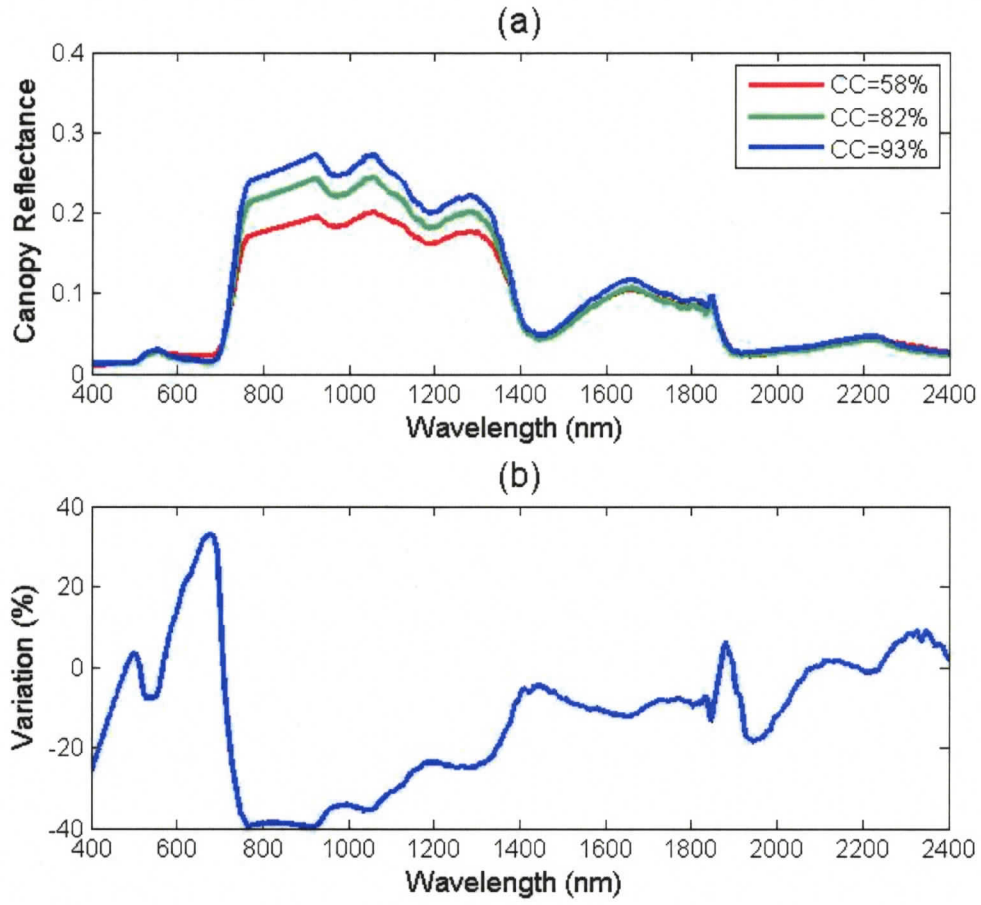

Figure 6.1.3 (a) Canopy reflectance simulated by FRT model with canopy closure (CC) of 58%, 82%, and 93%; (b) Variations (%) of simulated canopy reflectance with canopy closure changing from 58% to 93%.

6.1.4 Ground Vegetation

Figure 6.1.4 shows the response of canopy reflectance to variation in LAI of ground vegetation under different levels of canopy closure. For each level of canopy closure, the LAI of ground vegetation changes from 1 to 6. In general, the influence of ground LAI on canopy reflectance decreases as the canopy closure increases. In the visible region

around 700 nm, ground LAI has weak effect on canopy reflectance when canopy closure is less than 50%. In the NIR region, the influence of ground LAI is the strongest.

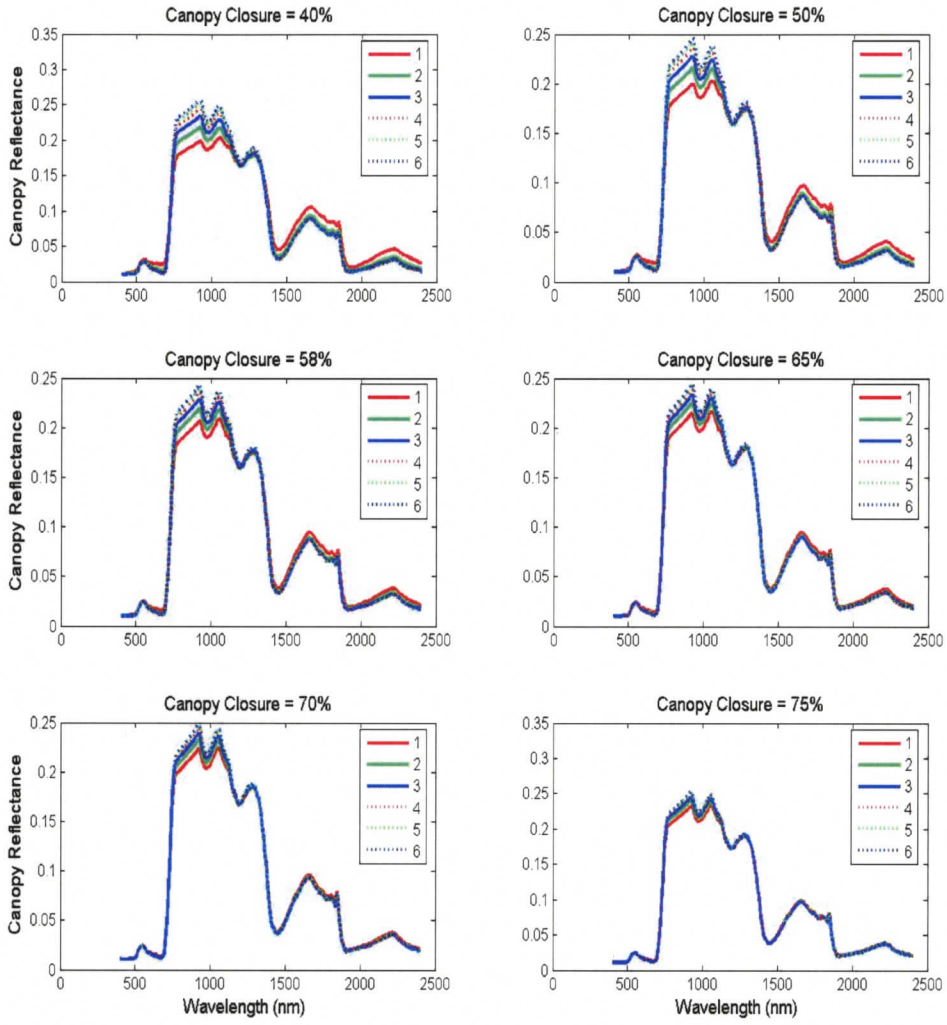

Figure 6.1.4 Response of canopy reflectance to variation in LAI of ground vegetation under different levels of canopy closure.

The signal of ground LAI is still significant when the canopy closure reaches 65%. In the SWIR region, when canopy closure is low (<50%), the ground LAI has relatively larger

influence in the SWIR-2 than the SWIR-1. When canopy closure is larger than 75%, the effect of ground LAI almost disappears.

Figure 6.1.5 demonstrates the response of canopy reflectance to variation in FMC of ground vegetation under different levels of canopy closure. FMC of ground vegetation changes from 80% to 240%. When canopy closure is less than 50%, ground FMC has effects in the NIR and whole SWIR region. When canopy closure is larger than 50%, the influence of ground FMC is very small.

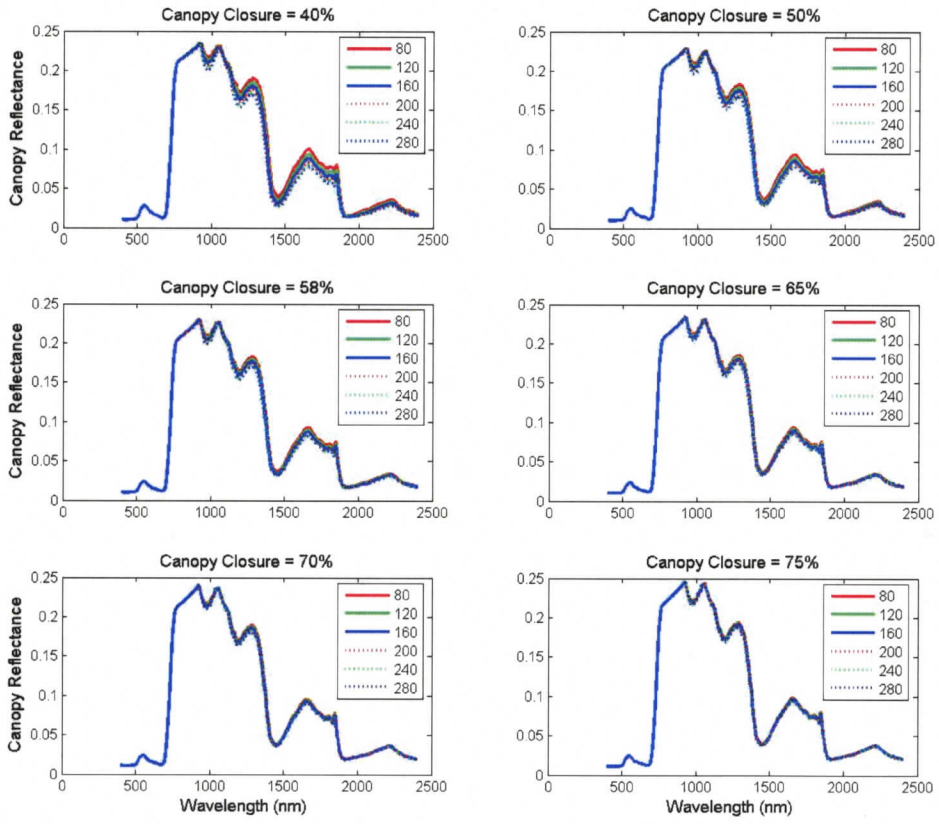

Figure 6.1.5 Response of canopy reflectance to variation in FMC of ground vegetation under different levels of canopy closure.

6.1.5 Soil

The coefficients for the first two Price's vector [94] are S_1 and S_2. Generally, the first vector explains about 60-90% variability of the natural surface. S_1 represents the brightness level of soil [75]. From Figure 6.1.6, we can see that S_1 has a very strong effect on canopy reflectance over the spectrum from 400 nm to 2400 nm when canopy closure is low. Even when the canopy closure is high (> 65%), the effect of S_1 is still strong in the NIR and SWIR-1 region. When canopy closure is larger than 70%, the effect of S_1 is almost negligible in the SWIR-2 region.

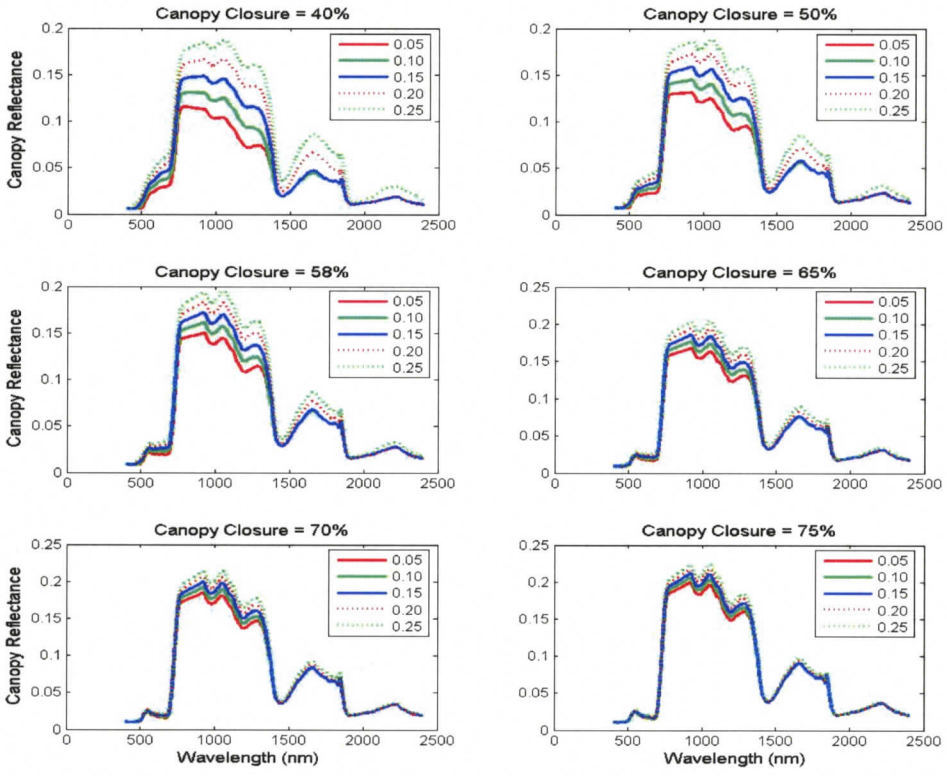

Figure 6.1.6 Response of canopy reflectance to variation in soil brightness (S_1) under different levels of canopy closure.

There is no good physical interpretation of S_2. Figure 6.1.7 shows that S_2 has very a strong effect on the SWIR region, especially in the SWIR-2 part. But in the NIR region around water absorption band 970 nm, the effect of S_2 is very weak. As canopy closure increases, the influence of S_2 decreases.

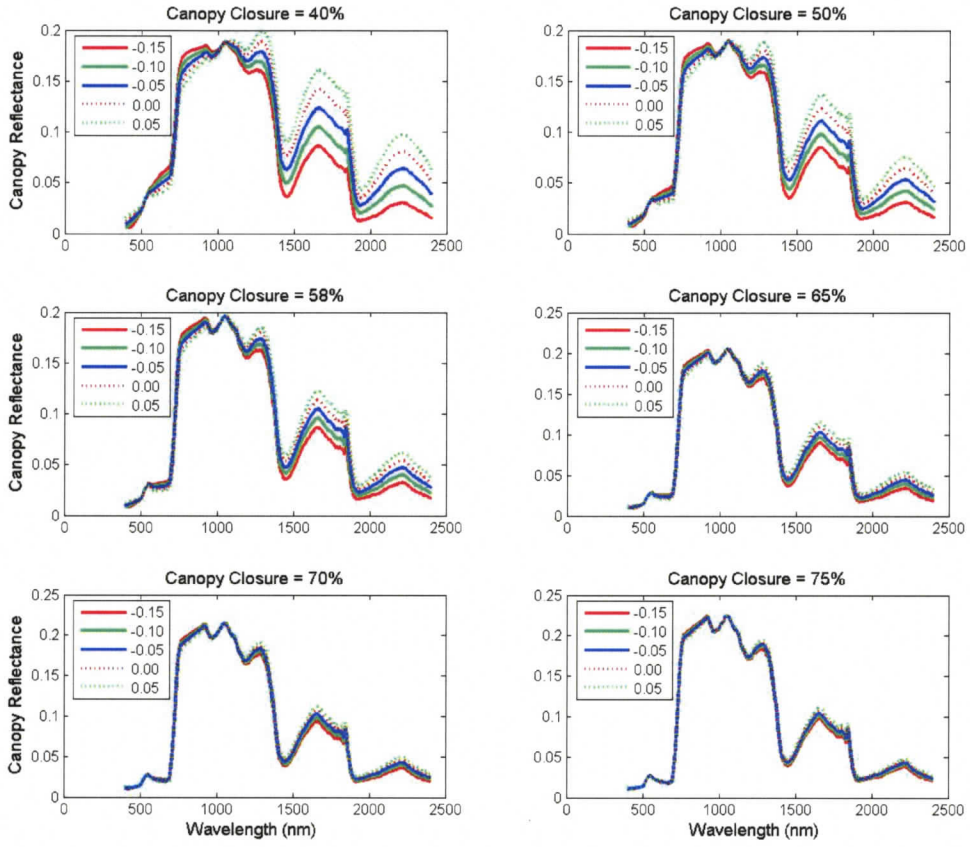

Figure 6.1.7 Response of canopy reflectance to variation in S_2 under different levels of canopy closure.

6.2 FMC from Water Index Methods

The vegetation indices that are potentially related to leaf water content are the normalized difference vegetation index (NDVI), water index (WI), normalized difference water index (NDWI), and moisture stress index (MSI). This section presents results using these indices to compute FMC.

The NDVI index is usually calculated by the vegetation reflectance at the NIR and visible region. The formula is:

NDVI = (NIR – Visible) / (NIR + Visible)

The NDVI responds to variations in amount of green biomass, chlorophyll content and leaf water stress [95]. The NDVI saturates in high biomass situations and is not a good indicator of biophysical features in dense forests [96, 97]. However, NDVI anomaly, which is defined as the difference between the average NDVI for a particular month of a given year and the long term average NDVI for the same month, could be used as an indicator of drought [98]. Therefore, we tested the performance of NDVI in estimating FMC. We expected that NDVI saturation would give poor correlations for FMC. In this study, we used 807 nm for the NIR and 664 nm for the Visible.

The WI index developed by Penuelas et al. [35, 36] was defined as WI = R970/R900, where R970 is the reflectance at the liquid water absorption band 970 nm and R900 is the reflectance at reference band 900 nm. Serrano et al. [47] used the WI index to map

vegetation water content with AVIRIS imagery and found that WI was affected not only by water content, but also by canopy structure and viewing geometry.

In a theoretical study, Gao [34] proposed the NDWI index to monitor vegetation water content by combining reflectance at 860 nm (a reference band) and 1240 nm (a liquid water absorption band) and demonstrated its potential applicability for canopy-level water content estimation. The value for NDWI is given by:

$$NDWI = (R860 - R1240) / (R860 + R1240)$$

In a simulation study, Zarco-Tejada and Ustin [99] showed the dependency of NDWI on canopy LAI.

The moisture stress index (MSI) was developed by Rock et al. [100]. It is a simple ratio between reflectance in the SWIR (sensitive to water content) to that in the NIR (sensitive to changes in leaf internal structure). Generally, it is derived from Landsat TM bands TM5 and TM4 on reflectance at 1600 nm (R1600) and 820 nm (R820):

$$MSI = R1600/R820$$

MSI is also sensitive to canopy LAI since it utilizes the reflectance in the SWIR region and even was used to estimate LAI in some studies [70, 101]. Compared to NDVI, SWIR-based water indices have been found more sensitive to leaf area and water content in closed canopies and saturate at higher LAI (larger than 3) [102-104].

In this study, we used the four indices to estimate FMC (both current and non-current) and evaluate their accuracy for different stands. Tables 6.1 and 6.2 contain the regression

coefficients (R^2 value) of each index. Water indices did not provide accurate estimates for most of the stands. Three water indices (WI, MSI, and NDWI) worked for estimating non-current FMC of plots with tree height in class [28.5, 37.4]. Among them (Figures 6.2.1-6.2.3), WI gave the best performance with R^2 of 0.56.

Table 6.1 Regression coefficients of current FMC retrieved by different vegetation indices for different stand parameters. (*)

Plots \ Indices	NDVI	MSI	WI	NDWI
All plots	0	0	0	0
DF plots	0.07	0.12	0.10	0.10
CC > 45%	0	0.02	0.02	0.02
CC > 55%	0	0.02	0.02	0.02
CC > 65%	0.06	0.06	0	0.02
28.5<H<37.4	0	0	0	0
19.5<H<28.4	0.14	0.09	0.05	0.05
H>28.4	0	0	0	0
H>37.4	0	0.02	0.11	0

* DF=Douglas-fir; CC=canopy closure; H=tree height (m); from 3rd row, only Douglas-fir plots.

Table 6.2 Regression coefficients of non-current FMC retrieved by different vegetation indices for different stand parameters. (*)

Plots \ Indices	NDVI	MSI	WI	NDWI
All plots	0.05	0.05	0.06	0.05
DF plots	0.01	0.10	0.13	0.09
CC > 45%	0.00	0.14	0.17	0.11
CC > 55%	0.00	0.14	0.17	0.11
CC > 65%	0.00	0.00	0.04	0.02
28.5<H <37.4	0.13	**0.40**	**0.56**	**0.50**
19.5<H<28.4	0.11	0.06	0.02	0.04
H>28.4	0.00	0.20	0.26	0.21
H>37.4	0.10	0.08	0.00	0.07

* DF=Douglas-fir; CC=canopy closure; H=tree height (m); from 3rd row, only Douglas-fir plots.

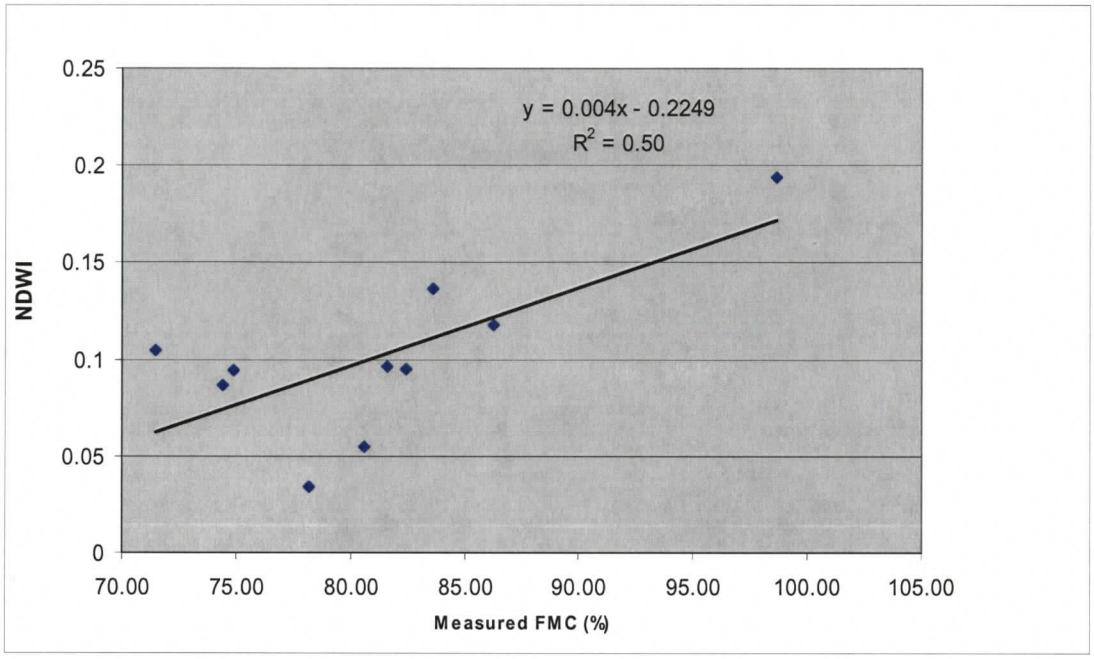

Figure 6.2.1 Correlation between NDWI and measured FMC (% of dry matter, non-current) for Douglas-fir plots with tree height (m) in the range of [28.5, 37.4].

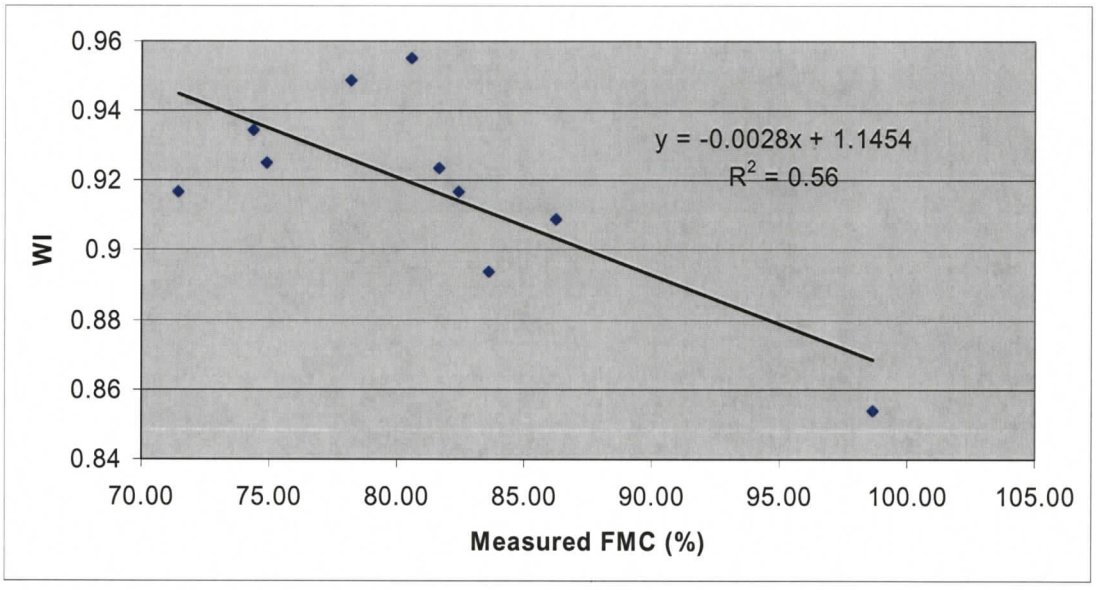

Figure 6.2.2 Correlation between WI and measured FMC (% of dry matter, non-current) for Douglas-fir plots with tree height (m) in the range of [28.5, 37.4].

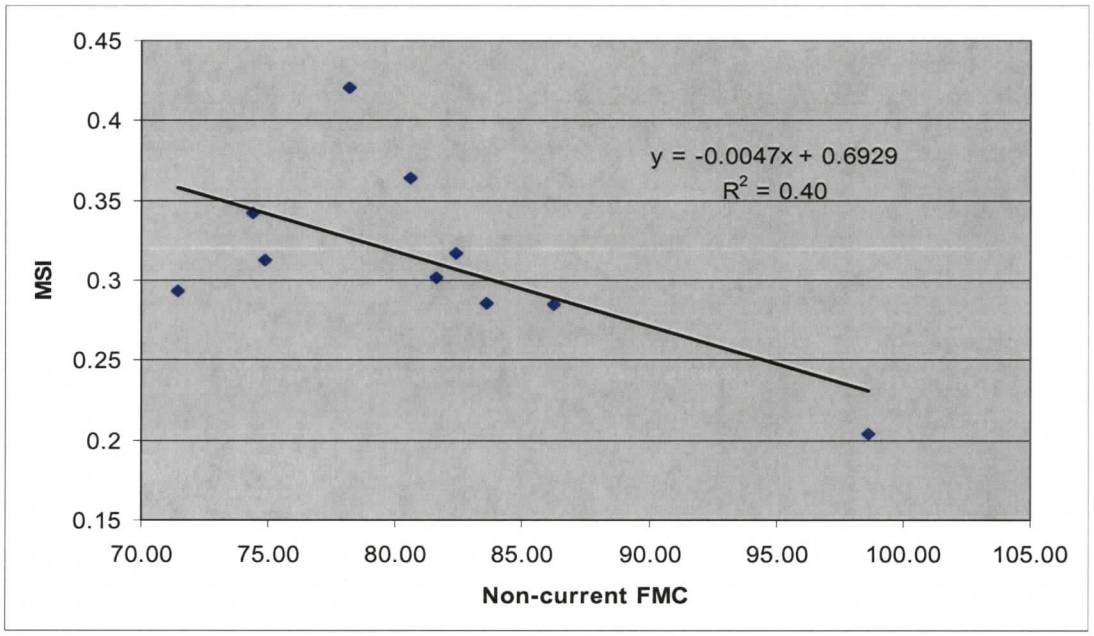

Figure 6.2.3 Correlation between MSI and measured FMC (% of dry matter, non-current) for Douglas-fir plots with tree height (m) in the range of [28.5, 37.4].

6.3 FMC from LUT Method

6.3.1 1-D LUT with FMC free

In this experiment, a one-dimensional lookup table (1-D LUT) was generated by the FRT model with FMC changing from 80% to 220% and all other variables fixed. Median values were used for canopy structural parameters. Tree height, stem density, DBH and NDM were set to be 33 m, 1016 trees/ha, 27.2 cm, and 24.99 kg/tree respectively. Sun zenith angle, which corresponds to the AVIRIS acquisition time of 20:06:00 GMT on August 10, 2001 over GVWD, was 33.4 degrees. Since we concentrate in this thesis on closed canopies, ground vegetation effects were minimal and were not included. The four liquid water absorption bands centered at 970 nm, 1190 nm, 1450nm and 1650 nm were used separately in computing the merit function. The 1650 nm band gives the best result. When tree height (H) is larger than 28.4 m, the regression coefficient (R^2 value) between the retrieved FMC and field measured FMC is 0.10 for Douglas-fir dominant plots (Figure 6.3.1) and 0.11 for pure Douglas-fir plots (Figure 6.3.2). When H is greater than 37.4 m, the accuracy is much better. The R^2 value is 0.48 for Douglas-fir dominant plots and 0.60 for pure Douglas-fir plots (Figures 6.3.3-4). This experiment suggests that we should allow tree height to be a variable to consider the variations in the canopy structure, especially LAI. In the following figures (Figures 6.3.3-6.3.16), significance levels of the correlations measured by the p-value were also calculated.

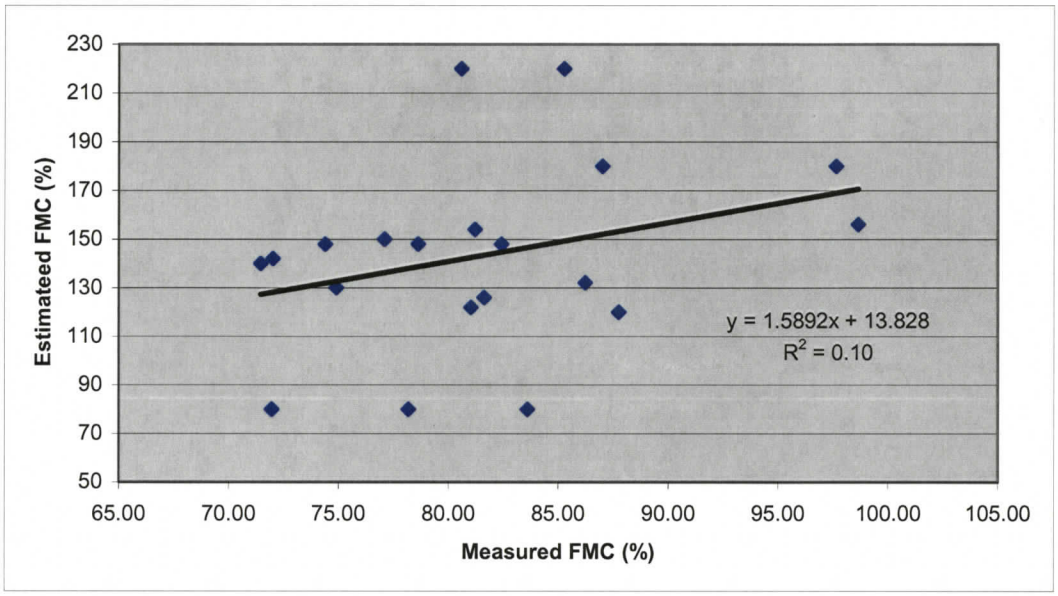

Figure 6.3.1 Comparison between estimated and field measured FMC (% of dry matter) over Douglas-fir dominant plots with tree height larger than 28.4 m. A 1-D lookup table generated by the FRT model was used for retrieval. The band at 1650 nm was used in computing the merit function.

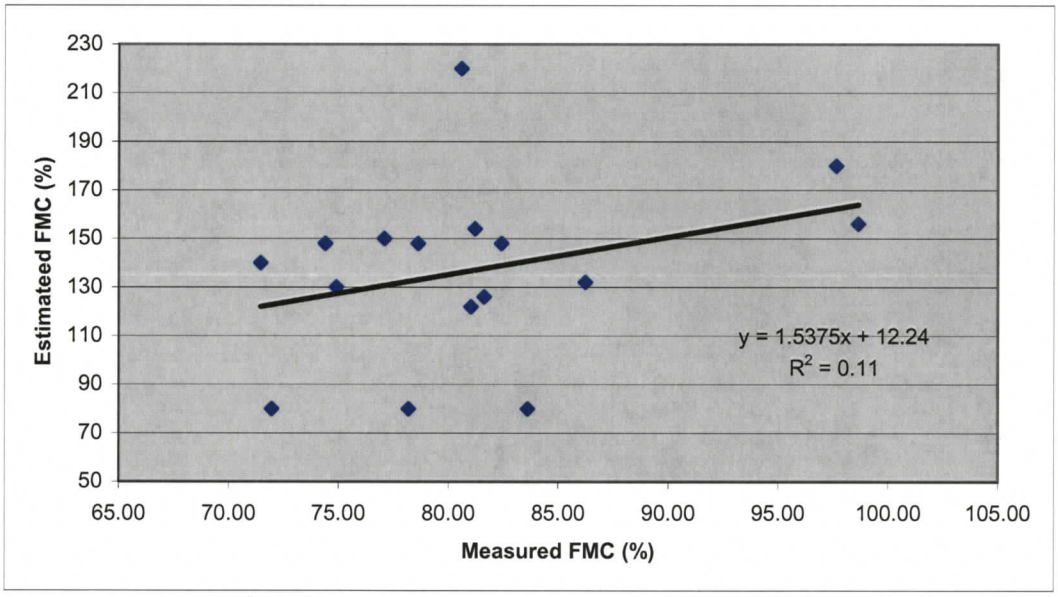

Figure 6.3.2 Comparison between estimated and field measured FMC (% of dry matter) over pure Douglas-fir plots with tree height larger than 28.4 m. A 1-D lookup table generated by the FRT model was used for retrieval. The band at 1650 nm was used in computing the merit function.

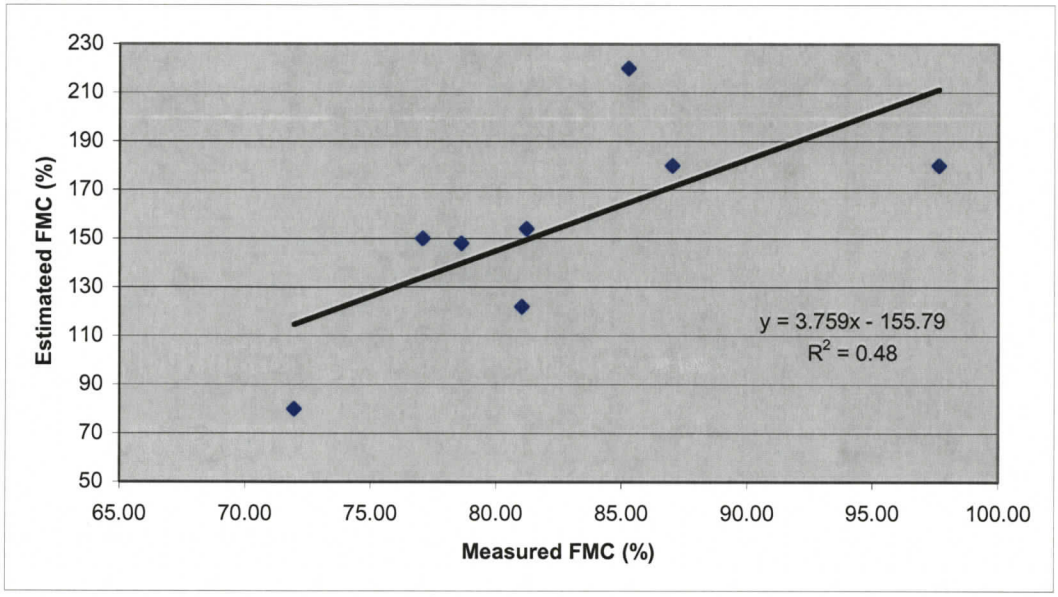

Figure 6.3.3 Comparison between estimated and field measured FMC (% of dry matter) over Douglas-fir dominant plots with tree height larger than 37.4 m ($p < 0.05$). A 1-D lookup table generated by the FRT model was used for retrieval. The band at 1650 nm was used in computing the merit function.

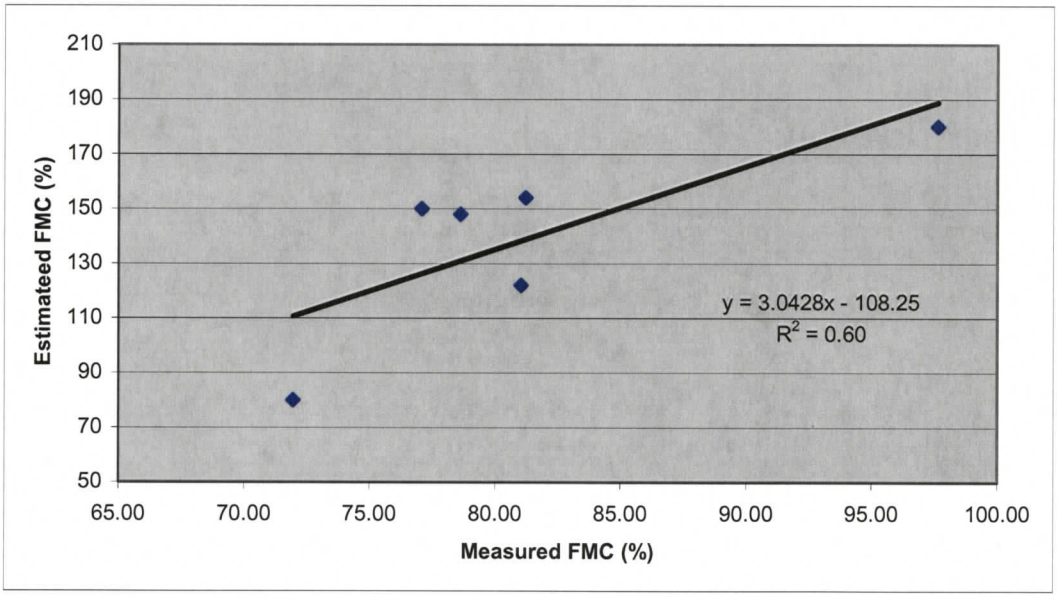

Figure 6.3.4 Comparison between estimated and field measured FMC (% of dry matter) over pure Douglas-fir plots with tree height larger than 37.4 m ($p < 0.05$). A 1-D lookup table generated by the FRT model was used for retrieval. The band at 1650 nm was used in computing the merit function.

6.3.2 2-D LUT with FMC and Tree Height Free

In this experiment, we generate a 2-dimensional lookup table (2-D LUT) by changing FMC for five tree height classes. For each tree height class, structural parameters were computed using formulas discussed in Section 4.3.2. The range of FMC is [90%, 212.5%] with an interval of 2.5%. The values of H for the five classes are 15 m, 24 m, 33m, 42 m, and 51 m.

First, we use the canopy reflectance at 1192 nm and 1650 nm to compute the merit function. As seen from sensitivity analysis in Section 6.1, 1192 nm is sensitive to both water content and canopy closure and 1650 nm is only sensitive to water content but not to canopy closure. When tree height is less than 28.4 m, R^2 is poor since most plots have canopy closure less than 55%. When tree height is larger than 28.4 m, all plots have canopy closure higher than 55%. Figures 6.3.5 and 6.3.6 show that R^2 is about 0.26 for Douglas-fir dominant plots and slightly high (0.32) for pure Douglas-fir plots. When tree height is larger than 37.4 m, the performance is much better. R^2 is 0.57 for Douglas-fir dominant plots (Figure 6.3.7) and 0.65 for pure Douglas-fir plots (Figure 6.3.9) though with few samples. If we remove the plots with CC less than 56%, we get a slightly better result (Figure 6.3.8) for Douglas-fir dominant plots.

In this experiment, by changing tree height, we implicitly consider LAI effects. When trees are taller than 37.4 m, performance is the best because most plots fall in age

between 100 and 250 years, at which Pacific coast Douglas-fir stands typically attain mature conditions and exhibit structural homogeneity, i.e., LAI variation is smaller. We also use 900 nm to compute the merit function. It gives a slightly better accuracy (R^2 = 0.60) than only using 1192 nm and 1650 nm for Douglas-fir dominant plots with height larger than 37.4 m (Figure 6.3.10).

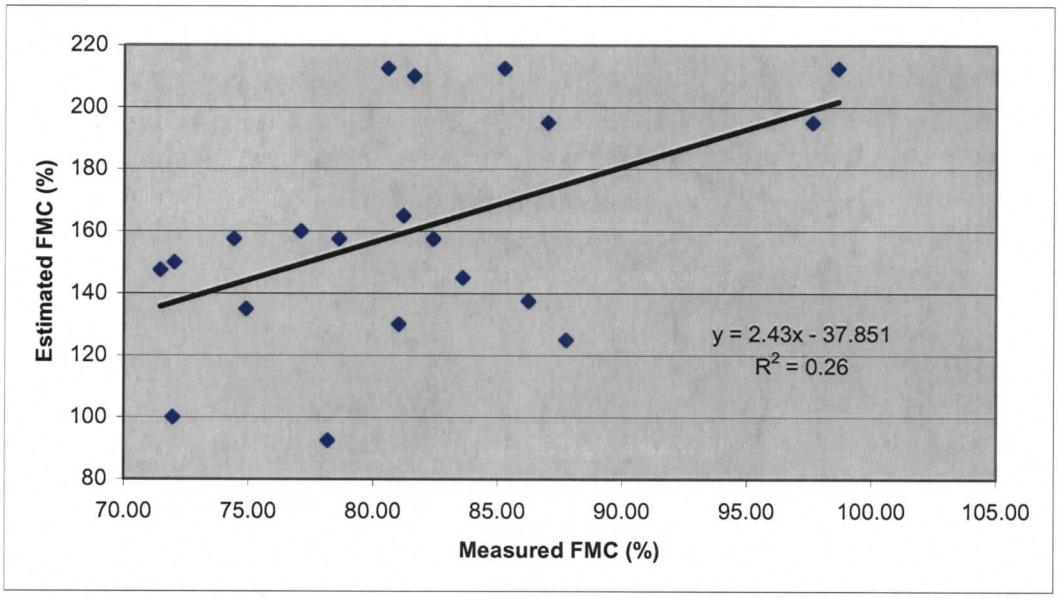

Figure 6.3.5 Comparison between estimated and field measured FMC (% of dry matter) over Douglas-fir dominant plots with tree height larger than 28.4 m ($p < 0.05$). A 2-D lookup table generated by the FRT model was used for retrieval. The bands at 1192 and 1650 nm were used in computing the merit function.

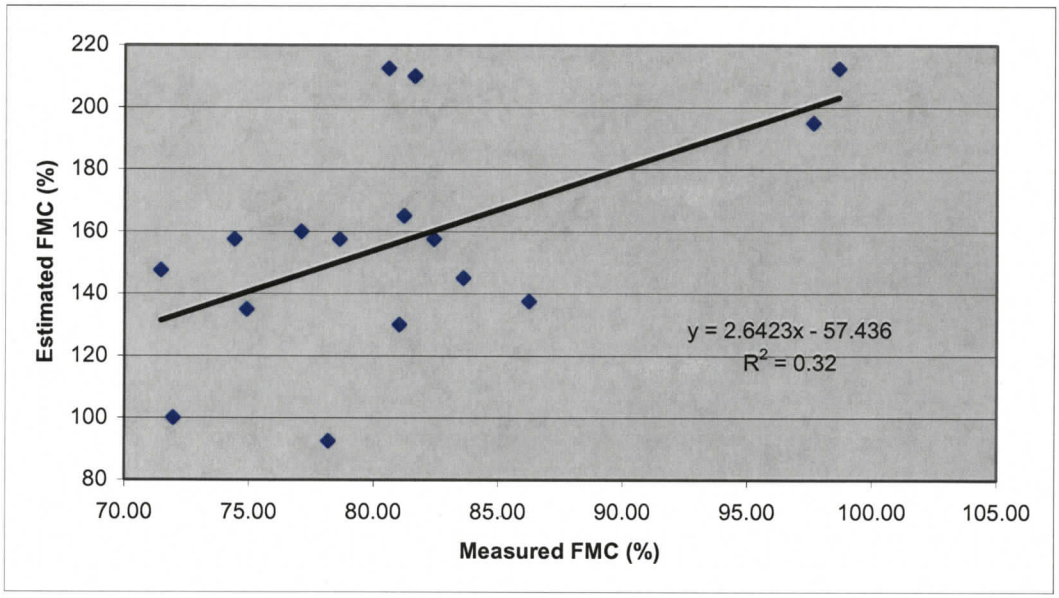

Figure 6.3.6 Comparison between estimated and field measured FMC (% of dry matter) over pure Douglas-fir plots with tree height larger than 28.4 m ($p < 0.05$). A 2-D lookup table generated by the FRT model was used for retrieval. The bands at 1192 and 1650 nm were used in computing the merit function.

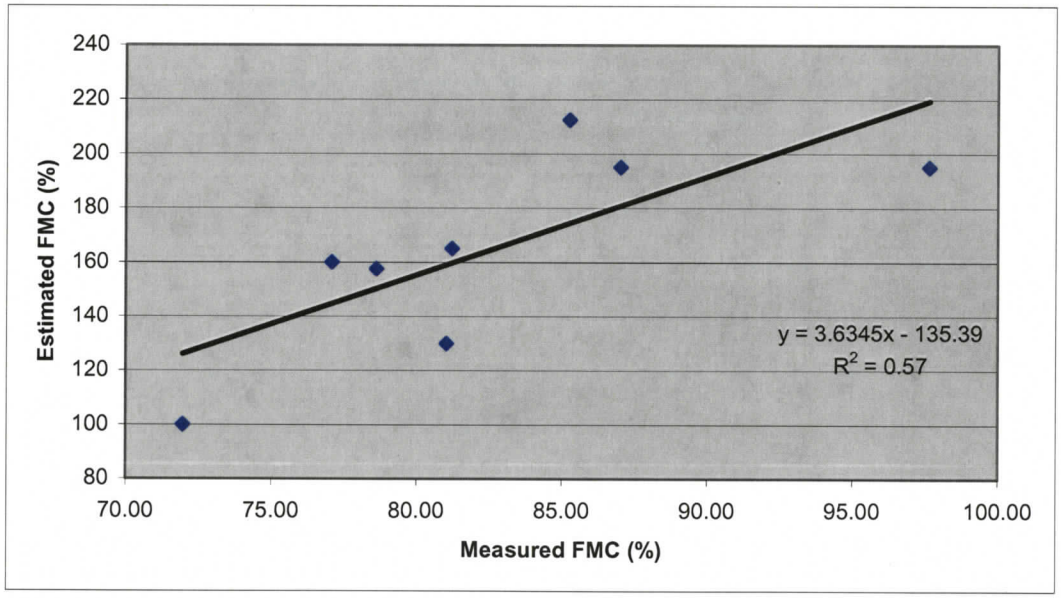

Figure 6.3.7 Comparison between estimated and field measured FMC (% of dry matter) over Douglas-fir dominant plots with tree height larger than 37.4 m ($p < 0.05$). A 2-D lookup table generated by the FRT model was used for retrieval. The bands at 1192 and 1650 nm were used in computing the merit function.

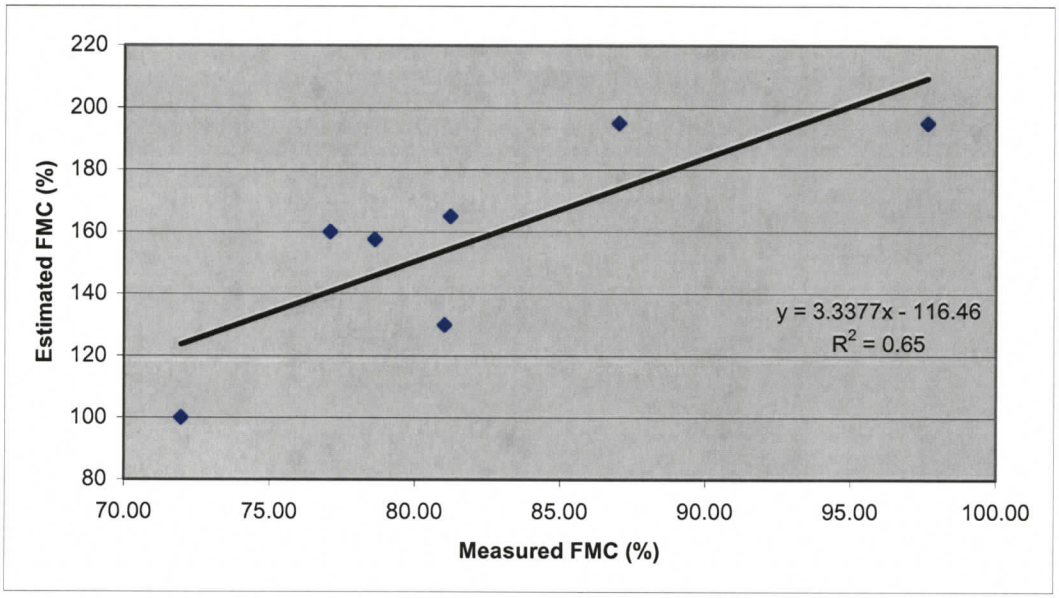

Figure 6.3.8 Comparison between estimated and field measured FMC (% of dry matter) over Douglas-fir dominant plots with tree height larger than 37.4 m and canopy closure greater than 55% ($p < 0.05$). A 2-D lookup table generated by the FRT model was used for retrieval. The bands at 1192 and 1650 nm were used in computing the merit function.

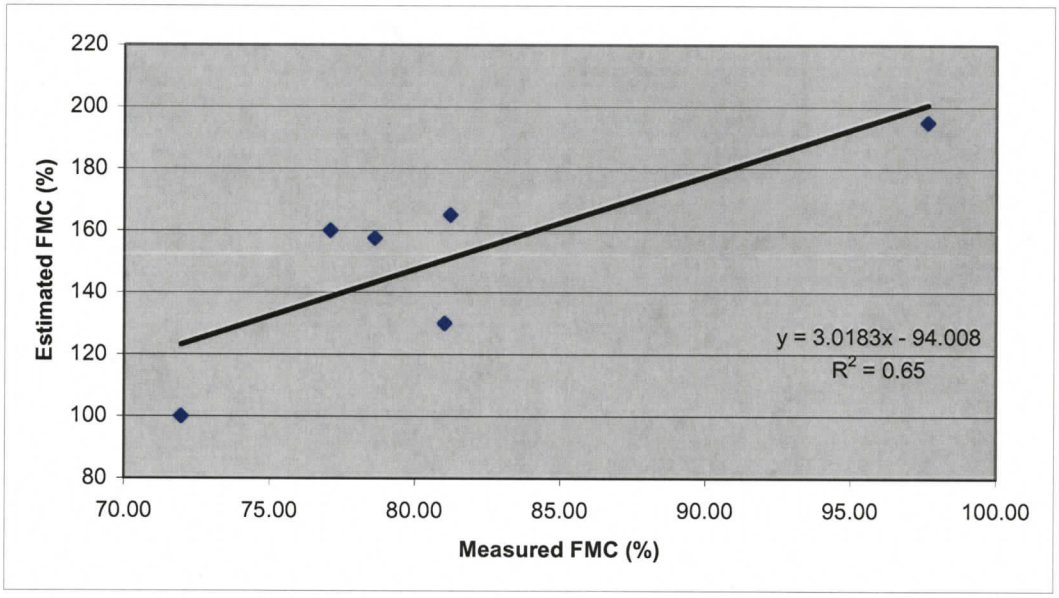

Figure 6.3.9 Comparison between estimated and field measured FMC (% of dry matter) over pure Douglas-fir plots with tree height larger than 37.4 m ($p < 0.05$). A 2-D lookup table generated by the FRT model was used for retrieval. The bands at 1192 and 1650 nm were used in computing the merit function.

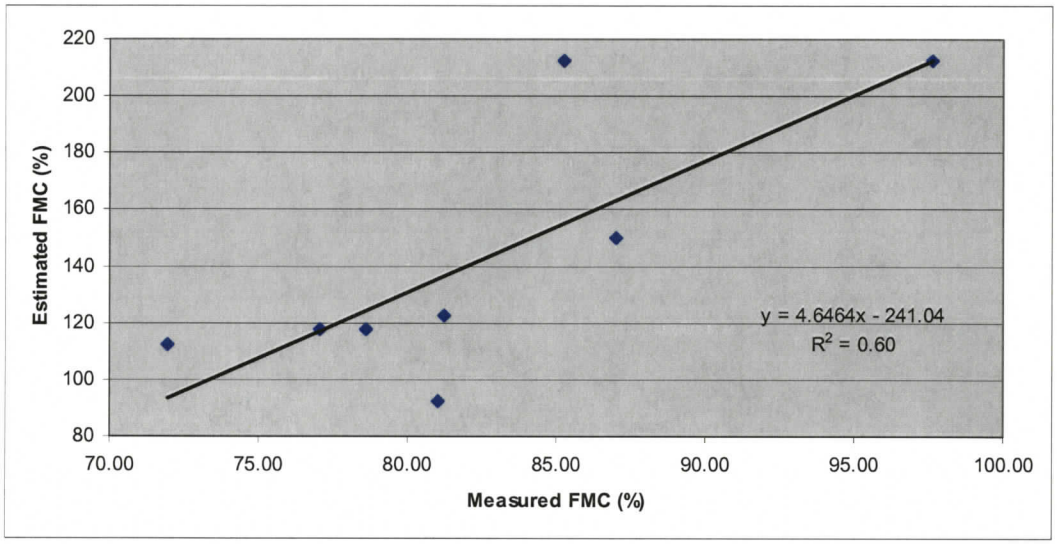

Figure 6.3.10 Comparison between estimated and field measured FMC (% of dry matter) over Douglas-fir dominant plots with tree height larger than 37.4 m ($p < 0.05$). A 2-D lookup table generated by the FRT model was used for retrieval. The bands at 900, 1192, and 1650 nm were used in computing the merit function.

6.3.3 3-D LUT with FMC, tree height and LAI free

In this experiment, a 3-dimensional lookup table (3-D LUT) was generated by the FRT model and used to retrieve FMC from the AVIRIS images. FMC, tree height (H), and LAI (by changing NDM) are the three free parameters. FMC changes in the range of [80%, 220%]. As in the above experiment, five tree height classes were used. For each H, in order to keep canopy closure high, we used the upper bound value of stem density derived from the Tree and Stand Simulator (TASS) [84, 85] and the corresponding DBH. For each H, a reference NDM value was computed by the formula for foliage biomass (Equation 4.3.4). By changing NDM centered at the reference value, we explicitly freed LAI. The AVIRIS-equivalent canopy reflectances were simulated at the following wavelengths: 606, 664, 702, 807, 865, 903, 974, 1192, 1452, 1652 nm. Table 6.3 shows the values of the main canopy structural parameters for the FRT model.

Noise levels of the AVIRIS data, ground measured FMC, and uncertainties of model inversion were also analyzed to help assess the accuracy and certainty of the system predictions. Figure 6.3.11 shows mean AVIRIS spectra of all Douglas-fir dominant plots (48 plots) and the standard errors of the mean, which are the standard deviations divided by the square root of the number of samples. We divided the pure Douglas-fir plots into two groups, one with tree heights larger than 28.5 m ("tall group", 16 plots) and another less than 28.5 m ("short group", 13 plots). The short group trees have higher standard deviation of FMC (11.0%) than the group with tall trees (7.8%). However, as shown in Figure 6.3.12 and Figure 6.3.13, plots with short trees have smaller variations in reflectance than plots with tall trees.

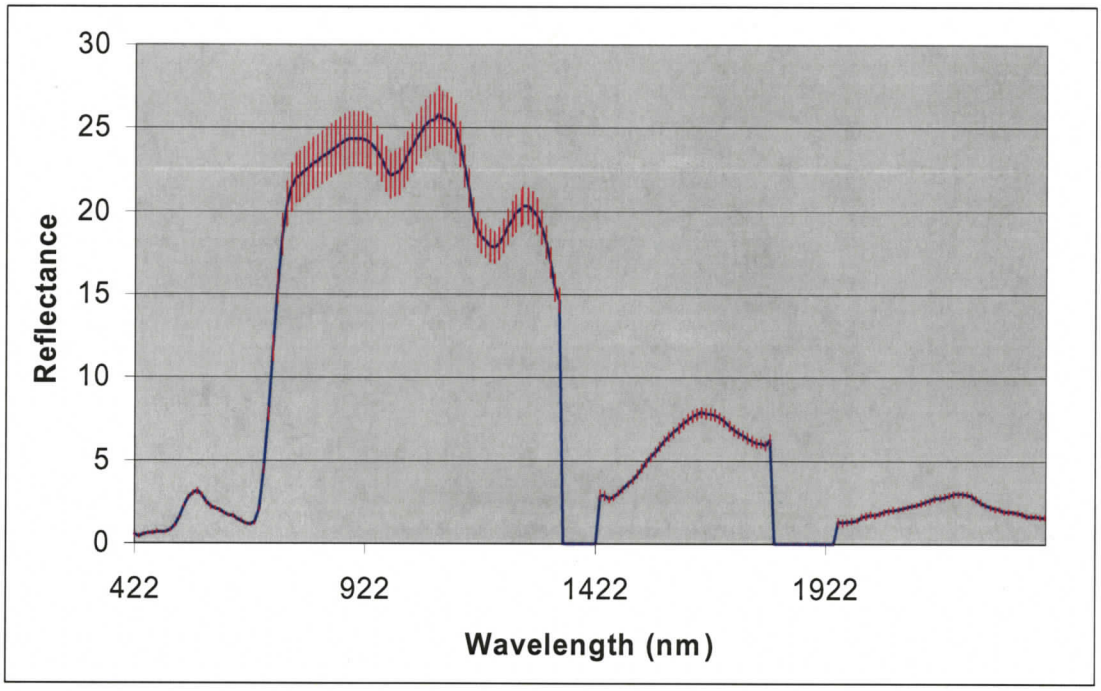

Figure 6.3.11 Mean spectra of all Douglas-fir dominant plots (Extracted from AVIRIS image). Error bars are +/- (standard errors of the mean) multiplied by 1.96 corresponding to the confidence level for the mean of samples equal to 95%. The number of plots was 48.

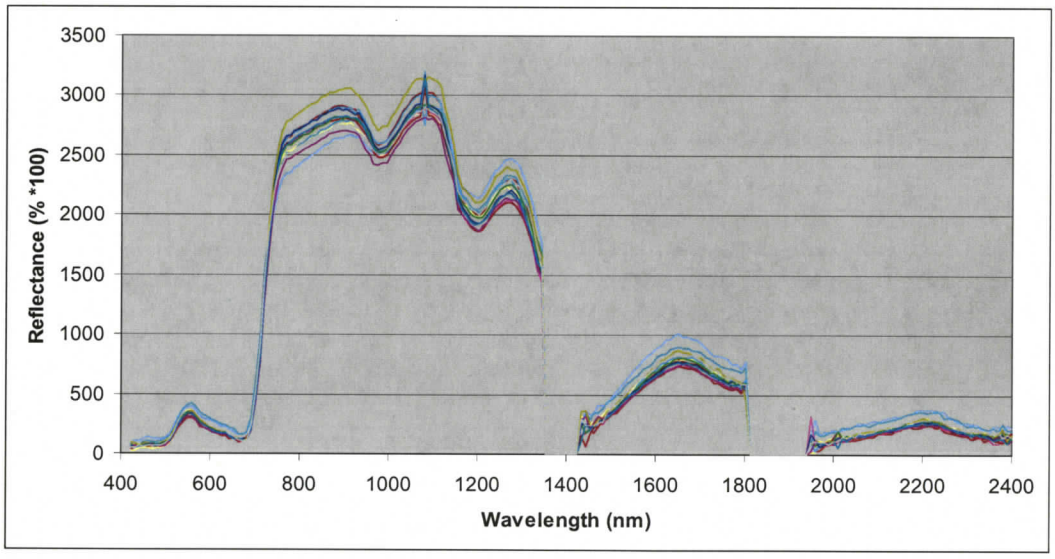

Figure 6.3.12 AVIRIS spectra of pure Douglas-fir plots with tree heights less than 28.4 m. The number of plots was 13.

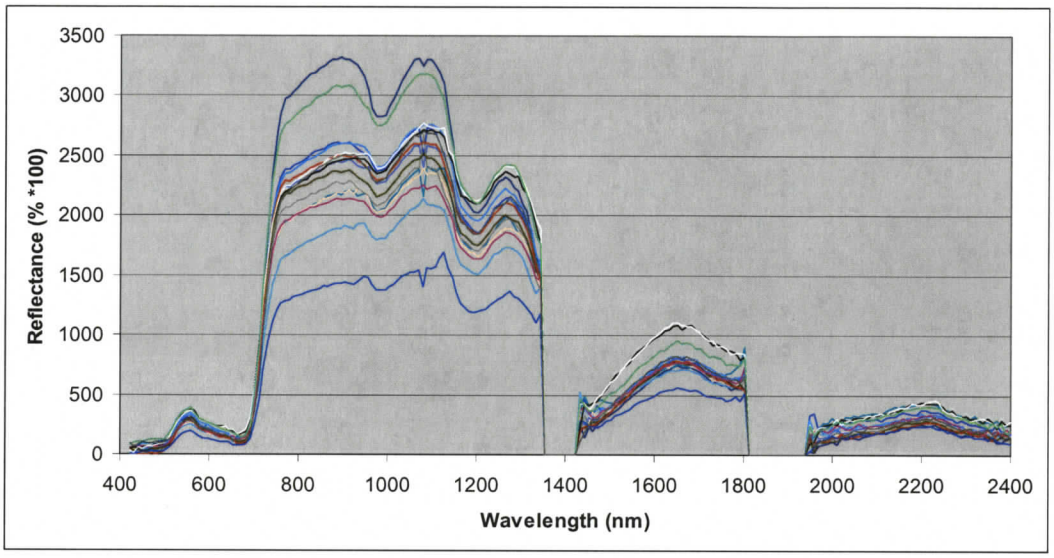

Figure 6.3.13 AVIRIS spectra of pure Douglas-fir plots with tree height larger than 28.4 m. The number of plots was 16.

The standard errors of the mean of FMC for each plot was computed from the ground measurements obtained in 2000, which contain ten samples for each plot. In order to compute the uncertainty of the model inversion, ten model states having the smallest merit functions were considered as possible solutions. Their standard errors of the mean were computed from the uncertainty of the inversion. The error bars for the uncertainties of inversion and ground measurements of FMC were computed from the standard errors of the mean multiplied by 1.96 which corresponds to confidence level of 95%. They are shown in the following figures (Figures 6.3.14-6.3.16).

As shown in Figures 6.3.14 and 6.3.15, the performance does not improve significantly for both Douglas-fir dominant plots and pure Douglas-fir plots with tree height larger than 28.4 m. But for plots with trees taller than 37.4 m, 3-D LUT (Figure 6.3.16) gave

better results ($R^2 = 0.74$) than 2-D LUT. For most plots, the uncertainties of model inversion were less than 6% with confidence level of 95%.

Table 6.3 Canopy structural parameters for generating 3-D LUT by the FRT model

H (m)	SD (trees/ha)	DBH (cm)	NDM (kg/tree)	LAI	CC (%)
15	3781	9.9	[1.0, 6.0]	[1.3, 3.7]	61
24	2002	17.0	[3.0, 14.0]	[2.1, 9.6]	69
33	1016	27.2	[8.0, 32.0]	[2.8, 11.2]	75
42	636	37.3	[13.0, 54.0]	[2.8, 11.8]	78
51	433	47.6	[20.0, 80.0]	[3.0, 11.9]	80

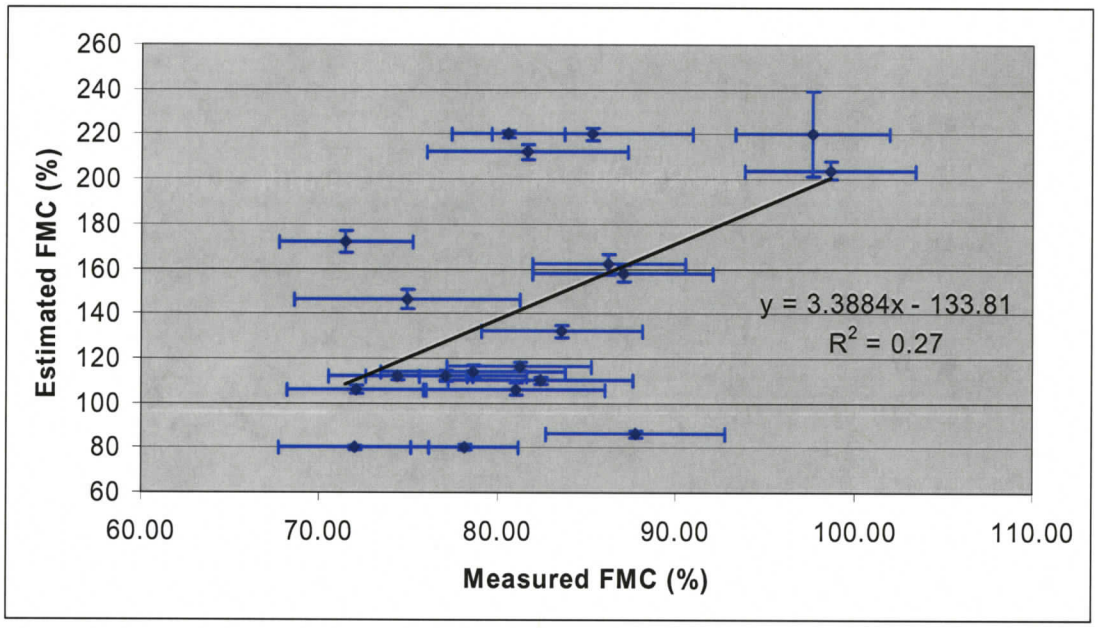

Figure 6.3.14 Comparison between estimated and field measured FMC (% of dry matter) over Douglas-fir dominant plots with tree heights larger than 28.4 m. A 3-D lookup table generated by the FRT model was used for retrieval. Bands at 903, 1192, and 1650 nm were used in computing the merit function. Error bars represent the uncertainties related to the ground measurements and model inversion, respectively. The R^2 value of 0.27 is not useful for this group of trees.

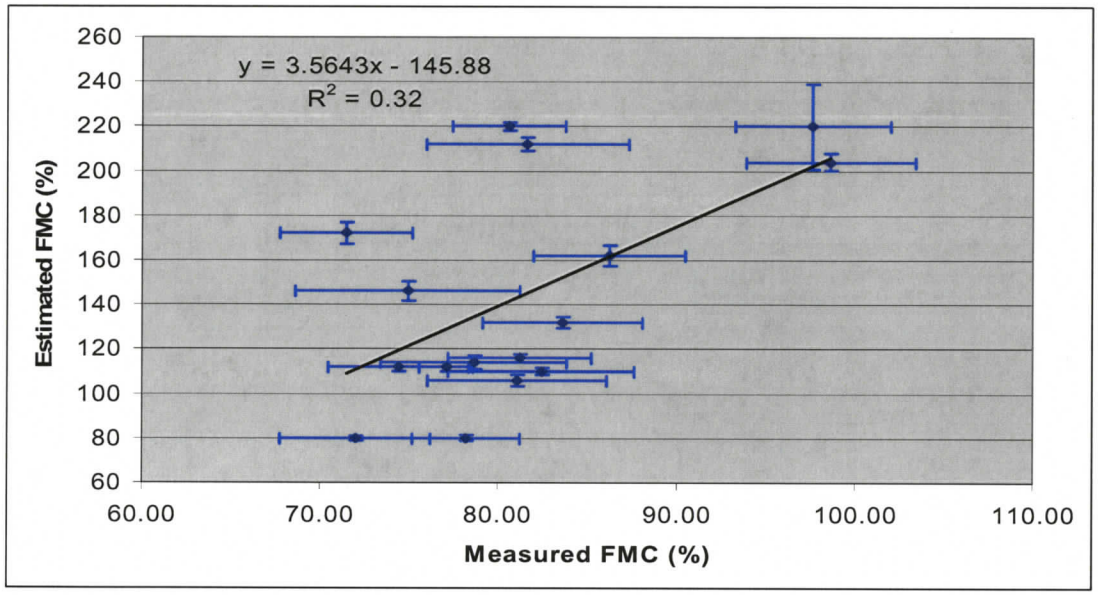

Figure 6.3.15 Comparison between estimated and field measured FMC (% of dry matter) over pure Douglas-fir plots with tree heights larger than 28.4 m. A 3-D lookup table generated by the FRT model was used for retrieval. Bands at 903, 1192, and 1650 nm were used in computing the merit function. Error bars represent the uncertainties related to the ground measurements and model inversion, respectively. The R^2 value for this group of trees is 0.32 with $p < 0.01$.

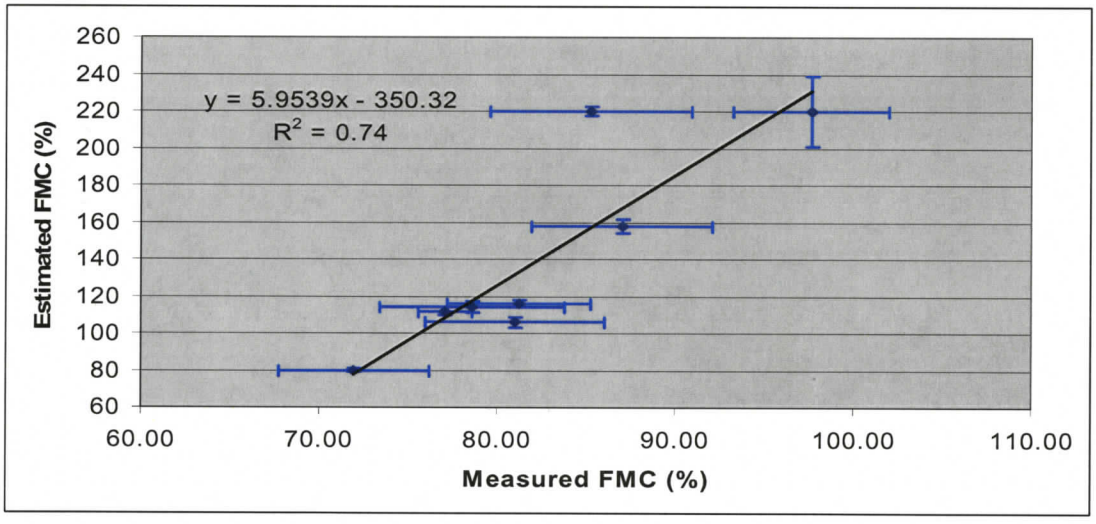

Figure 6.3.16 Comparison between estimated and field measured FMC (% of dry matter) over Douglas-fir dominant plots with tree heights larger than 37.4 m. A 3-D lookup table generated by the FRT model was used for retrieval. Bands at 903, 1192, and 1650 nm were used in computing merit function. Error bars represent the uncertainties related to the ground measurements and model inversion, respectively. The R^2 value is 0.74 for this group of trees with $p < 0.01$.

Chapter 7

Conclusions and Future Work

7.1 Conclusions

The objective of this thesis was to investigate whether with remote sensing data we can estimate fuel moisture content of forest. The research further aimed to design and develop a computing system that was capable of generating lookup tables for different forest scenes and retrieving fuel moisture content of Douglas-fir forests from remote sensing data.

These goals were achieved by:

- Analyzing the effects of FMC, LAI, canopy closure, ground vegetation and soil on canopy reflectance.
- Identifying wavelength regions that are sensitive to fuel moisture content.
- Configuring canopy structural parameters based on forest dynamics of Douglas-fir.
- Generating lookup tables by a forest radiative transfer model, FRT.
- Estimating the FMC of Douglas-fir dominant pixels from AVIRIS images using lookup table inversion method.
- Assessing accuracy through comparison of estimated FMC with field measurements and results from water indices.

- Implementing the Fuel Moisture Content Mapping System (FMAS) by integrating the FRT model and a set of new modules.
- Implementing a canopy reflectance simulation module to simulate canopy reflectance for different forest scenes with various biochemical and biophysical conditions.
- Implementing a LUT generation module to integrate simulated canopy reflectance into AVIRIS-equivalent reflectance and generate lookup tables.
- Implementing a FMC estimation module including a graphical user interface (GUI) to retrieve fuel moisture content (FMC) for Douglas-fir dominant pixels in a hyperspectral image.

The core methodology used in this study was based on the use of radiative transfer models. The physical approach allows for the analysis of the effects of various biophysical and biochemical variables on canopy reflectance. It also allows the creation of lookup tables that are used to retrieve the forest variables of interest.

The sensitivity analysis has shown that the canopy water content is a function of the foliage water content and canopy LAI. It is essential to separate the contributions of LAI and FMC. Canopy closure has a very strong influence on canopy reflectance in the NIR and SWIR-1 region and is weak in other parts. The wavelength region around 900 nm helps to differentiate canopy closures.

Limited field measurements were used to test the performance of the physical approach and water indices. Water indices (WI, MSI, and NDWI) only worked for estimating non-current FMC of plots with tree height in the class of [28.5m, 37.4m]. Among them, WI gave the best performance with R^2 of 0.56. The physical approach achieved overall better results than the water index method. For pure Douglas-fir plots with H > 28.4 m, the physical approach achieved R^2 of 0.34. For plots with trees taller than 37.4 m, the 3-D LUT gave R^2 of 0.74.

This thesis has shown that the physical approach works much better than water indices in estimating fuel moisture content for Douglas-fir forests with high canopy closure. It provides an alternative way to determine forest biophysical and biochemical variables over large areas.

7.2 Areas of Future Work

As a result of this research, several concerns emerged for future investigation. These areas include:

- Model validation at leaf and canopy level

  Many parameters in the leaf and canopy model were configured either through forest dynamic relationships or though peer-reviewed literature. Further research is required to validate the leaf and canopy models for species of interest both in the laboratory and the field.

- Direct estimation of canopy structural variables, specifically tree height and LAI

  Most of the canopy structural variables (DBH, crown length, crown radius) are related to tree height. This work shows the effects of LAI on canopy reflectance and it is critical to identify LAI in order to better estimate FMC. It is not easy to separate the contribution of LAI from FMC by just using optical sensor data. Further investigation of the potential use of active sensors to retrieve tree structural variables could help resolve this problem.

- More detailed field measurements

  Small sample size limits the possible inversion experiments and makes it hard to draw solid conclusions. To fully explore the potential of physical approaches, more detailed and rich field measurements would be required. These measurements include:

  (1) Variables at leaf level (FMC, Chlorophyll concentration), canopy level (tree height, canopy closure, LAI, DBH, crown radius, crown length, BAI), and landscape level (stem density).

  (2) EM spectra between 400 and 2500 nm of branch, trunk, ground vegetation and soil.

- Computing speed for generating LUT and estimating FMC

The computing performance will decrease as the dimensions of the lookup table increase. Future investigation should be undertaken to improve the computing performance for operationally retrieving foliage water content from remote sensing data. Parallel computing can be used to solve this problem. For example, all the processors on a Linux cluster or a high performance workstation can be used to run the same code on different parts of the image simultaneously.

Bibliography

1. Jensen, J.R., Remote Sensing of the Environment. Prentice Hall Series in Geographic Information Science, ed. K.C. Clarke. 2000, Upper Saddle River, Prentice Hall, 544.
2. Jacquemoud, S. and S.L. Ustin. Application of radiative transfer models to moisture content estimation and burned land mapping. in *Proc. 4th International Workshop on Remote Sensing and GIS Applications to Forest Fire Management*, Ghent, Belgium, vol., pp. 3-12, 2003.
3. Radke, L.E., T.L. Clark, J.L. Coen, C.A. Walther, R.N. Lockwood, P.J. Riggen, J.A. Brass, and R.G. Higgins. The WildFire Experiment (WiFE): Observations with Airborne Remote Sensors. Canadian Journal of Remote Sensing, vol. 26(5), pp. 406-477, 2000.
4. Amiro, B.D., J.B. Todd, B.M. Wotton, K.A. Logan, M.D. Flannigan, B.J. Stocks, J.A. Mason, D.L. Martell and K.G. Hirsch. Direct carbon emissions from Canadian forest fires, 1959-1999. Canadian Journal of Forest Research, vol. 31, pp. 512-525, 2001.
5. Tansey, K., Gregoire, J-M., Stroppiana, D., Sousa, A., Silva, J.M.N., Pereira, J.M.C., Boschetti, L., Maggi, M., Brivio, P.A., Fraser, R., Flasse, S., Ershov, D., Binaghi, E., Graetz, D. and Peduzzi, P. Vegetation burning in the year 2000: Global burned area estimates from SPOT VEGETATION data. Journal of Geophysical Research - Atmospheres, vol. 109, D14S03, DOI:10.1029/2003JD003598, 2004.
6. Dasgupta, S., J.J. Qu, and X. Hao. Design of a Fire Susceptibility Index for fire risk monitoring. IEEE Transactions on Geoscience and Remote Sensing, vol. 3(1), pp. 140-144, 2006.
7. Stow, D., J. Kaiser, and M. Niphadkar. MODIS-derived visible atmospheric resistant Index for monitoring chaparral moisture content. International Journal of Remote Sensing, vol. 26(17), pp. 3867-3873, 2005.
8. Bowyer, P. and F.M. Danson. Sensitivity of spectral reflectance to variation in live fuel moisture content at leaf and canopy level. Remote Sensing of Environment, vol. 92, pp. 297-308, 2004.
9. Carlson, J.D., and R. E. Burgan. Review of user needs in operational fire danger estimation: the Oklahoma example. International Journal of Remote Sensing, vol. 24(8), pp. 1601-1620, 2003.
10. Chuvieco, E., I. Aguado, and A.P. Dimitrakopoulos. Conversion of fuel moisture content values to ignition potential for integrated fire

danger assessment. Canadian Journal of Forest Research, vol. 34, pp. 2284-2293, 2004.

11. Wotton, B.M. and D.L. Martell. A lightning fire occurrence model for Ontario. Canadian Journal of Forest Research, vol. 35, pp. 1389-1401, 2005.
12. Flannigan, M.D., B.J. Syocks, and B.M. Wotton. Climate change and forest fires. The Science of the Total Environment, vol. 262, pp. 221-229, 2000.
13. Viegas, D.X., J. Pinol, M.T. Viegas, and R. Ogaya. Estimating live fine fuels moisture content using meteorologically based indices. Internal Journal of Wildland Fire, vol. 10, pp. 223-240, 2001.
14. Castro, F.X., A. Tudela, and M.A. Sebastia. Modeling moisture content in shrubs to predict fire risk in Catalonia (Spain). Agricultural and Forest Meteorology, vol. 116, pp. 49-59, 2003.
15. Kotchenova, S., N. Shabanov, Y. Knyazikhin, A. Davis, R. Dubayah, and R. Myneni. Modeling lidar waveforms with time-dependent stochastic radiative transfer theory for remote estimations of forest biomass. Journal of Geophysical Research, vol. 108(No. D15, 4484, 10.1029/2002JD003288), 2003.
16. Verbesselt, J., S. Fleck, and P. Coppin, Estimation of fuel moisture content towards Fire Risk Assessment: A review, in Forest Fire Research & Wildland Fire Safety, Viegas, Editor. 2002, Millpress, Rotterdam.
17. Ceccato, P., S. Flasse, S. Tarantola, S. Jacquemoud, and J. Gregoire. Detecting vegetation leaf water content using reflectance in the optical domain. Remote Sensing of Environment, vol. 77, pp. 22-33, 2001.
18. Danson, F.M. and P. Bowyer. Estimating live fuel moisture content from remotely sensed reflectance. Remote Sensing of Environment, vol. 92, pp. 309-321, 2004.
19. Roberts, D.A., P.E. Dennison, M.E. Gardner, Y. Hetzel, S.L. Ustin, and C.T. Lee. Eavluation of the potential of Hyperion for fire danger assessment by comparison to the airborne visible/infrared imaging spectrometer. IEEE Transactions on Geoscience and Remote Sensing, vol. 41(6), pp. 1297-1310, 2003.
20. Chuvieco, E., D. Riano, I. Aguado, and D. Cocero. Estimation of fuel moisture content from multitemporal analysis of Landsat Thematic Mapper reflectance data: application in fire danger assessment. International Journal of Remote Sensing, vol. 23(11), pp. 2145-2162, 2002.

21. Van Wagner, C.E. Seasonal variation in moisture content of Eastern Canadian tree foliage and the possible effect on crown fires. in Departmental Publication no. 1204. 1967, Forestry Branch, Canada.
22. Chandler, C., P. Cheney, P. Thomas, L. Trabaud, and D. Williams, Fire in forestry: forest fire behavior and effects. 1983, New York, John Wiley & Sons, 450.
23. Van Wagner, C.E. Conditions for the start and spread of crown fire. Canadian Journal of Forest Research, vol. 7, pp. 23-34, 1977.
24. Hopkins, W.G. and N.P.A. Huner, Introduction to plant physiology. 3rd ed. 2004, John Wiley & Sons, 560.
25. Canadian Forest Service, N.R.C., Canadian Forest Fire Danger Rating System. http://cwfis.cfs.nrcan.gc.ca/en/background/bi_FDR_summary_e.php.
26. Carter, G.A. Primary and secondary effects of water content of the spectral reflectance of leaves. American Journal of Botany, vol. 78, pp. 916-924, 1991.
27. Irons, J.R., K.J. Ranson, D. Williams, R. Irish, and F. Huegel. An off-nadir-pointing imaging spectrometerfor terrestrial ecosystem studies. IEEE Transactions on Geoscience and Remote Sensing, vol. 29, pp. 66-74, 1991.
28. Green, R.O., M.L. Eastwood, C.M. Sarture, T.G. Chrien, M. Aronsson, B.J. Chippendale, J.A. Faust, B.E. Pavri, C.J. Chovit, M. Solis, M.R. Olah, and O. Williams. Imaging spectroscopy and the airborne visible/infrared imaging spectrometer (AVIRIS). Remote Sensing of Environment, vol. 65, pp. 227-248, 1998.
29. Anger, C., S. Achal, T. Ivanco, S. Mah, R. Price, and J. Busler. Extended operational capabilities of casi. in *Proc. The Second International Airborne Remote Sensing Conference*, San Francisco, California, vol., pp. 124-133, 1996.
30. Neiville, R.A., N. Rowlands, R. Marois, and I. POwell. SFSI: Canada's first airborne SWIR imaging spectrometer. Canadian Journal of Remote Sensing, vol. 21, pp. 328-336, 1995.
31. Ceccato, P., N. Gobron, S. Flasse, B. Pinty, and S. Tarantola. Designing a spectral index to estimate vegetation water content from remote sensing data: Part 1 Theoretical approach. Remote Sensing of Environment, vol. 82, pp. 188-197, 2002.
32. Saltelli, A., S. Tarantola, and K.P.-S. Chan. A quantitative model independent method for global sensitivity analysis of model output. (American Statistical Association and the American Society for Quality) Technometrics, vol. 41(1), pp. 39-56, 1999.

33. Jacquemoud, S., C. Bacour, H. Loilve, and J.P. Frangi. Comparison of four radiative transfer models to simulate plant canopies reflectance: Direct and inverse mode. Remote Sensing of Environment, vol. 74, pp. 471-481, 2000.
34. Gao, B.C. NDVI - a normalized difference water index for remote sensing of vegetation liquid water from space. Remote Sensing of Environment, vol. 58, pp. 257-266, 1996.
35. Penuelas, J., I. Filella, C. Biel, L. Serrano, and R. Save. The reflectance at the 950-970 nm region as an indicator of plant water status. International Journal of Remote Sensing, vol. 14, pp. 1887-1905, 1993.
36. Penuelas, J., I. Filella, L. Serrano, and R. Save. Cell wall elasticity and Water Index (R970 nm /R900 nm) in wheat under different nitrogen availabilities. International Journal of Remote Sensing, vol. 17, pp. 373-382, 1996.
37. Penuelas, J., J. Pinol, R. Ogaya, and I. Filella. Estimation of plant water concentration by the reflectance Water Index WI (R900/R970). International Journal of Remote Sensing, vol. 18, pp. 2869-2875, 1997.
38. Penuelas, J. and Y. Inoue. Reflectance indices indicative of changes in water and pigment contents of peanut and wheat leaves. Photosynthetica, vol. 36(3), pp. 355-360, 1999.
39. Gao, B.C. and A.F.H. Goetz. Retrieval of equivalent water thickness and information related to biochemical components of vegetation canopies from AVIRIS data. Remote Sensing of Environment, vol. 52, pp. 144-162, 1995.
40. Goodenough, D.G., H. Chen, A. Dyk, T. Han, S. McDonald, M. Murdoch, K.O. Niemann, J. Pearlman, and C. West. EVEOSD Forest Information Products from AVIRIS and Hyperion. in *Proc. IGARSS' 03*, Toulouse, France, vol. I, pp. 284-287, 2003.
41. Dawson, T.P., O.J. Curran, and S.E. Plummer. The biochemical decomposition of slash pine needles from reflectance spectra using neural networks. International Journal of Remote Sensing, vol. 19, pp. 1433-1438, 1998.
42. Jacquemoud, S., F. Baret, B. Andrieu, F.M. Danson, and K. Jaggard. Extraction of vegetation biophysical parameters by inversion of the PROSPECT + SAIL models on sugar beet canopy reflectance data. Applications to TM and AVIRIS sensors. Remote Sensing of Environment, vol. 52, pp. 162-172, 1995.

43. Jacquemoud, S., S.L. Ustin, J. Verdebout, G. Schmuck, G. Andreoli, and B. Hosgood. Estimating leaf bio-chemistry using the PROSPECT leaf optical properties model. Remote Sensing of Environment, vol. 56, pp. 194-202, 1996.
44. Gastellu-Etchegorry, S.P., F. Gascon, and P. Esteve. An interpolation procedure for generalizing a look-up table inversion method. Remote Sensing of Environment, vol. 87, pp. 55-71, 2003.
45. Ustin, S.L., D.A. Roberts, J. Pinzon, S. Jacquemoud, M. Gardner, G. Scheer, C.M. Castaneda, and A. Palacios-Orueta. Estimating canopy water content of chaparral shrubs using optical methods. Remote Sensing of Environment, vol. 65, pp. 280-291, 1998.
46. Riano, D., P. Vaughan, E. Chuvieco, P.J. Zarco-Tejada, and S.L. Ustin. Estimation of fuel moisture content by inversion of radiative transfer models to simulate equivalent water thickness and dry matter content: analysis at leaf and canopy level. IEEE Transactions on Geoscience and Remote Sensing, vol. 43(4), pp. 819-825, 2005.
47. Serrano, L., S.L. Ustin, D.A. Roberts, J.A. Gamon, and J. Penuelas. Deriving water content of chaparral vegetation from AVIRIS data. Remote Sensing of Environment, vol. 74, pp. 570-581, 2000.
48. Ceccato, P., S. Flasse, and J. Gregoire. Designing a spectral index to estimate vegetation water content from remote sensing data: Part 2. Validation and application. Remote Sensing of Environment, vol. 82, pp. 198-207, 2002.
49. Chuvieco, E., I. Aguado, D. Cocero, and D. Riano. Design of an emperical index to estimate fuel moisture content from NOAA-AVHRR images in forest fire danger studies. International Journal of Remote Sensing, vol. 24(8), pp. 1621-1637, 2003.
50. Goodenough, D.G., A.S. Bhogal, A. Dyk, K.O. Niemann, T. Han, H. Chen, C. West, and C. Schmidt. Calibration of forest chemistry for hyperspectral analysis. in *Proc. IGARSS' 01*, Sidney, Australia, vol. I, pp. 52-56, 2001.
51. Research Systems, Inc. FLAASH Module User's Guide. 2005.
52. Dyk, A., D.G. Goodenough, A.S. Bhogal, J. Pearlman, and J. Love. Geometric correction and validation of Hyperion and ALI data for EVEOSD. in *Proc. IGARSS' 02*, Toronto, Ontario, Canada, vol. I, pp. 579-583, 2002.
53. Goodenough, D.G., H. Chen, A. Dyk, S. McDonald, M. Murdoch, K.O. Niemann, J. Pearlman, and C. West. Forest information products from AVIRIS and Hyperion. in *Proc. AVIRIS Workshop*, Pasadena, CA, vol., pp., 2003.

54. Green, A.A., Berman, M., Switzer, P, and Craig, M. D. A transformation for ordering multispectral data in terms of image quality with implications for noise removal. IEEE Transactions on Geoscience and Remote Sensing, vol. 26(1), pp. 65-74, 1988.
55. Schowengerdt, R.A., Techniques for Image Processing and Classification in Remote Sensing. 1983, New York, Academic Press.
56. Mather, P.M., Computer Processing of Remotely Sensed Images, An Introduction. 2 ed. 1989, New York, Wiley, 320.
57. Jacquemoud, S. and S.L. Ustin. Leaf optical properties: A state of the art. in *Proc. 8th International Symposium on Physical Measurements and Signatures in Remote Sensing*, Aussois, France, vol., pp. 223-232, 2001.
58. Jacquemoud, S. and F. Baret. Prospect: a model of leaf optical properties spectra. Remote Sensing of Environment, vol. 34, pp. 75-91, 1990.
59. Kimes, D., F. Nelson, M. Manry, and A. Fung. Attributes of neural networks for extracting continuous vegetation variables from optical and radar measurements. International Journal of Remote Sensing, vol. 19(14), pp. 2639-2663, 1998.
60. Barnsley, J., P. Lewis, S. O'Dwyer, M. Disney, P. Hobson, M. Cutter, and D. Lobb. On the potential of CHRIS-PROBA for estimating vegetation canopy properties from space. Remote Sensing Reviews, vol. 19(Special Issue: 2nd International Workshop on Multi-angular Measurements and Modelling), pp. 171-189, 2000.
61. Li, X. and A. Strahler. Geometrical-optical modeling of a conifer forest canopy. IEEE Transactions on Geoscience and Remote Sensing, vol. 23, pp. 705-721, 1985.
62. Li, X. and A. Strahler. Geometrical-optical bidirectional reflectance modeling of a coniferous forest canopy. IEEE Transactions on Geoscience and Remote Sensing, vol. 24, pp. 906-919, 1986.
63. Li, X. and A. Strahler. Geometrical-optical bidirectional reflectance modeling of the discrete-crown vegetation canopy: effect of crown shape and mutual shadowing. IEEE Transactions on Geoscience and Remote Sensing, vol. 30, pp. 276-292, 1992.
64. Goel, N.S., Inversion of Canopy reflectance models for estimation of biophysical parameters from reflectance data, in Theory and applications of optical remote sensing, Asrar, Editor. 1989, Wiley, New York, pp. 205-241.

65. Nilson, T. and A. Kuusk. A reflectance model for the homogenous plant canopy and its inversion. Remote Sensing of Environment, vol. 27, pp. 157-167, 1989.
66. Allen, W.A. Transmission of isotropic light across a dielectric surface in two and three dimensions. Journal of the Optical Society of America, vol. 63, pp. 664-666, 1973.
67. Govaerts, Y.M., S. Jacquemoud, M.M. Verstraete, and S.L. Ustin. Three-dimensional radiation transfer modeling in a dicotyledon leaf. Applied Optics, vol. 35, pp. 6585-6598, 1996.
68. Lewis, P. Three-dimensional plant modeling for remote sensing simulation studies using the botanical plant modeling system. Agronomie, vol. 19, pp. 185-210, 1999.
69. Kuusk, A. and T. Nilson. A directional multispectral forest reflectance model. Remote Sensing of Environment, vol. 72, pp. 244-252, 2000.
70. Rautiainen, M. Retrieval of leaf area index for a coniferous forest by inverting a forest reflectance model. Remote Sensing of Environment, vol. 99(3), pp. 295-303, 2005.
71. Rautiainen, M., P. Stenberg, T. Nilson, A. Kuusk, and H. Smolander. Application of a forest reflectance model in estimating leaf area index of Scots pine stands using Landsat-7 ETM reflectance data. Canadian Journal of Remote Sensing, vol. 29(3), pp. 314-323, 2003.
72. Rautiainen, M., P. Stenberg, T. Nilson, and A. Kuusk. The effect of crown shape on the reflectance of coniferous stands. Remote Sensing of Environment, vol. 89, pp. 41-52, 2004.
73. Bacour, C., J. Jacquemoud, M. Leroy, O. Hauteceur, M. Weiss, L. Prevot, N. Bruguier, and H. Chauki. Reliability of the estimation of vegetation characteristics by inversion of three canopy reflectance models on airborne POLDER data. Agronomie, vol. 22, pp. 555-565, 2002.
74. Kuusk, A. Monitoring of vegetation parameters on large areas by the inversion of a canopy reflectance model. International Journal of Remote Sensing, vol. 19(15), pp. 2893-2905, 1998.
75. Kuusk, A., Lang, M., and Nilson, T. Simulation of the reflectance of ground vegetation in sub-boreal forests. Agricultural and Forest Meteorology, vol. 126(1-2), pp. 33-46, 2004.
76. Pinty, B., J-L. Widlowski, M. Taberner, N. Gobron, M. M. Verstraete, M. Disney, F. Gascon, J.-P. Gastellu, L. Jiang, A. Kuusk, P. Lewis, X. Li, W. Ni-Meister, T. Nilson, P. North, W. Qin, L. Su, S. Tang, R. Thompson, W. Verhoef, H. Wang, J. Wang, G. Yan, and H. Zang.

Results from the second phase. Journal of Geophysical Research, vol. 109, D06210 10.1029/2003JD004252, 2004.

77. Vermote, E.F., D. Tanre, J.L. Deuze, M. Herman, and J.J. Morcrette. Second simulation of the satellite signal in the solar spectrum, 6S - An overview. IEEE Transactions on Geoscience and Remote Sensing, vol. 35, pp. 675-686, 1997.
78. Berk, A., L.S. Bernstein, G.P. Anderson, P.K. Acharya, D.C. Robertson, J.H. Chetwynd, and S.M. Adler-Golden. MODTRAN cloud and multiple scatteting upgrades with application to AVIRIS. Remote Sensing of Environment, vol. 65, pp. 367-375, 1998.
79. Dawson, T.P., P.J. Curran, and S.E. Plummer. LIBERRTY - modeling the effects of leaf biochemical concentration on reflectance spectra. Remote Sensing of Environment, vol. 65, pp. 50-60, 1998.
80. Vermote, E., D. Tanre, J.L. Deuze, M. Herman, and J.J. Morcrette. Second Simulation of Satellite Signal in the Solar Spectrum (6S). User Guide Version 0. 1994, GSFC, NASA.
81. Kuusk, A. A two-layer canopy reflectance model. Journal of Quantitative Spectroscopy and Radiative Transfer, vol. 71, pp. 1-9, 2001.
82. Verhoef, W. Light scattering by leaf layers with application to canopy reflectance modelling: the SAIL model. Remote Sensing of Environment, vol. 16, pp. 125-141, 1984.
83. Kuusk, A. and T. Nilson. FRT User Guide. 2005.
84. Mitchell, K.J. and I.R. Cameron. Managed stand yield tables for coastal Douglas-fir: initial density and precommercial thinning. in Land Management Report No. 31. 1985, Forest Research Branch, Ministry of Forests.
85. Mitchell, K.J. Simulation of the growth of even-aged stands of white spruce. in Yale Univ. School of Forestry Bull. 1969, Yale University: New Haven, CN. p. 48.
86. Nilson, T. Forest reflectance model as an interface between satellite images and forestry databases. in *Proc. Rogow' 99*, Rogow, Poland, vol., pp., 1999.
87. Marshall, J.D. and R.A. Monserud. Foliage height influences specific leaf area of three conifer species. Canadian Journal of Forest Research, vol. 33, pp. 164-170, 2003.
88. Combal, B., F. Baret, M. Weiss, A. Trubuil, D. Mace, A. Pragnere, R. Myneni, Y. Knyazikhin, and L. Wang. Retrieval of canopy biophysical variables from bidirectional reflectance using prior

information to solve the ill-posed inverse problem. Remote Sensing of Environment, vol. 84, pp. 1-15, 2002.

89. Kurz, F., O. Hellwich, and H. Ebner. Estimation of vegetation parameters from multispectral data using physical models and ground control measurements. Photogrammetris-Fernerkundung-Geoinformation, vol. 4, pp. 253-262, 2002.
90. Liang, S., Quantitative Remote Sensing of Land Surfaces. 2003, John Wiley and Sons, 534.
91. Weiss, M., F. Baret, R. Myneni, A. Pragnere, and Y. Knyazikhin. Investigation of a technique to estimate canopy biophysical variables from spectral and directional reflectance data. Agronomie, vol. 20, pp. 3-22, 2000.
92. Myneni, R.B., Y. Knyazikhin, Y. Zhang, Y. Tian, Y. Wang, A. Lotsch, J.L. Privette, J.T. Morisette, S.W. Running, R. Nemani, J. Glassy, and P. Votava. Modis Leaf Area Index (LAI) and Fraction of Photosynthetically Active Radiation Absorbed by Vegetation (fPAR) Product: Algorithm Theoretical Basis Document. 1999.
93. Kalluri, S.N.V., J. Jaja, D.A. Bader, Z. Zhang, J.R.G. Townshend, and H. Fallah-Adl. High performance computing algorithms for land cover dynamics using remote sensing data. International Journal of Remote Sensing, vol. 21(6 & 7), pp. 1513-1536, 2000.
94. Price, J. On the information Content of Soil Reflectance Spectra. Remote Sensing of Environment, vol. 33, pp. 113-121, 1990.
95. Treitz, P.M. and P.J. Howarth. Hyperspectral remote sensing for estimating biophysical parameters of forest ecosystems. Progress in Physical Geography, vol. 23, pp. 359-390, 1999.
96. Freitas, S.R., M.C.S. Mello, and C.B.M. Cruz. Relationships between forest structure and vegetation indices in Atlantic Rainforest. Forest Ecology and Management, vol. 218(1-3), pp. 353-362, 2005.
97. Huete, A.R., H.Q. Liu, and W.J.D. Van Leeuwen. The use of vegetation indices in forested regions: issues of linearity and saturation. in *Proc. IGARSS' 97*, Singapore, vol. 4, pp. 1966-1968, 1997.
98. NASA, Measuring Vegetation (NDVI & EWI). http://earthobservatory.nasa.gov/Library/MeasuringVegetation/measuring_vegetation_3.html.
99. Zarco-Tejada, P.J. and S.L. Ustin. Modeling canopy water content for carbon estimates from MODIS data at land EOS validation sites. in *Proc. IGARSS' 01*, vol. 1, pp. 342-344, 2001.
100. Rock, B.N., J.E. Vogelmann, D.L. Williams, A.F. Vogelmann, and T.

Hoshizaki. Remote detection of forest damage. Bioscience, vol. 36, pp. 439-445, 1986.

101. Eklundh, L., K. Hall, H. Eriksson, J. Ardo, and P. Pilesjo. Investigating the use of Landsat thematic mapper data for estimation of forest leaf area index in southern Sweden. Canadian Journal of Forest Research, vol. 29(3), pp. 349-362, 2003.
102. Chen, D., J. Huang, and T. J. Jackson. Vegetation water content estimation for corn and soybeans using spectral indices derived from MODIS near- and short-wave infrared bands. Remote Sensing of Environment, vol. 98, pp.225-236, 2006.
103. Anderson, M. C., C. M. U. Neale, F. Li, J. M. Norman, W. P. Kustas, H. Jayanthi, and J. Chavez. Upscaling ground observations of vegetation water content, canopy height, and leaf area index during SMEX02 using aircraft and Landsat imagery. Remote Sensing of Environment, vol. 92, pp.447-464, 2004.
104. Roberts, D. A., R. O. Green, and J. B. Adams. Temporal and spatial patterns in vegetation and atmospheric properties from AVIRIS. Remote Sensing of Environment, vol. 62, pp.223-240, 1997.

A.1 A sample input file for FRT

```
'DF'              : data set name
100                                   : stand age
1                                     : # size classes
*** files of refractive index and other tree classes:
'spectra/refrind.dat'
x0        xmin      xmax      dx                                              i
x0: value of the variable used in the forward simulation
xmin, xmax, dx are used in the inversion mode
'DF'                                  : species
f_ell                                 : crown form
.1        .01       .1        .01     : stand density, m-2                    1
25.00     10.       30.       2.      : tree height, m                        2
8.36      .5        10.       9.      : crown l,m ell V con                   3
12.64     .5        10.       1.      : cylinder                              4
2.51   2  5.        .3                : crown radius, m                       5
22.34     2.        25.       5.      : trunk diameter, cm                    6
6.39      .1        8.        8.      : m - total dry leaf weight, kg/tree    7
291.55    30.       180.      60.     : SLW - leaf weight per area, gm-2      8
.15       .01       1.        .05     : BAI/LAI                               9
1.49      .6        2.8       .05     : tree    distr.    param               10
.8        .5        .8        .2      : shoot   shading   coef                11
'prospect'                            : leaf optics model
3                                     : # of leaf components
.68   .3   1.   .2   'spectra/chlorp3.dat'   : c1, % of SLW, model component 1  12
250.  80.  300. 2.   'spectra/waterp3.dat'   : c2, % of SLW, model component 2  13
99.3  94.  99.8 20.  'spectra/drymatter.dat' : c3, % of SLW, model component 3  14
.01                                   : leaf str. param. - coefficient        24
1.                                    : refraction index ratio                25
.1                                    : shoot length, m                       26
'pineBark.dat'                        : file of branch reflectance
'pineBark.dat'                        : file of trunk reflectance
3                                     : crown layer number nz
*** Ground vegetation ***
.10       .01       6.        .3      : LAI2_ground, upper layer              27
.15       .02       .4        .05     : sl2_ground                            28
1.        .4        1.        .2      : sz2 - the Markov parameter            29
                                      (used to compute canopy geometry)
0.        .0        4.5       .5      : eln2 - -ln(1 - eps)                   30
90.       0.        90.       20.     : thm2 - modal leaf angle               31
                                      (above two parameters used to compute leaf distribution angle)
.9        .6        1.3       .2      : n_ratio2                              32
160.      80.       180.      30.     : SLW2(g/m^2)                           33
'prospect'                            : leaf optics model, upper layer
4                                     : # of leaf components
.4        .3        .8        .2      'spectra/chlorp3.dat'  : c1, % of SLW, model component 1  34
150.      120.      320.      20.     'spectra/waterp3.dat'  : c2, % of SLW, model component 2  35
99.6      94.       99.8      20.     'spectra/drymatter.dat' : c3, % of SLW, model component 3  36
.2        .0002     4.        .1      'spectra/brownpigm.dat' : c4, % of SLW, model component 4  37
.0112     .01       .05       .05                              : N2 (PROSPECT) – coefficient   46
.1        .01       1.        .3      : LAI1_ground, lower layer              47
.15       .02       .4        .05     : sl1_ground                            48
1.        .4        1.        .2      : sz1 - the Markov parameter            49
                                      (used to compute canopy geometry)
```

```
0.      .0      4.5     .5      : eln1 - -ln(1 - eps)                                   50
90.     0.      90.     20.     : thm1 - modal leaf angle                               51
                                (above two parameters used to compute leaf distribution angle)
.9      .6      1.3     .2      : n_ratio1                                              52
160.    80.     180.    30.     : SLW1(g/m^2)                                           53
'prospect'                      : leaf optics model, lower layer
4                               : # of leaf components
.4      .3      .8      .2      'spectra/chlorp3.dat' : c1, % of SLW, model component 1 54
150.    130.    320.    50.     'spectra/waterp3.dat' : c2, % of SLW, model component 2 55
99.6    94.     99.8    20.     'spectra/drymatter.dat' : c3, % of SLW, model component 3 56
.2      .0002   4.      .1      'spectra/brownpigm.dat' : c4, % of SLW, model component 4 57
.0112   .01     .05     .05     : N1 (PROSPECT) - coefficient     66
'price.dat'     45.             : file of Price' vectors, th*
.28     .05     .4      .07     : s1 - soil parameters                                  67
-.02    -.1     .1      .02     : s2                                                    68
.0      -.05    .05     .02     : s3                                                    69
.0      -.04    .04     .02     : s4                                                    70
*** 6S parameters ***
2       .70     .29     .0      .01     : iaer, c(n) - aerosol data (6S)
30.     .060                            : v, tau_aer(550) - visibility (6S)
1 : *ijob*: 0-single, 1-spectrum, 2-ad, 3-n_sun, 4,5-inversion (4-relat., 5-abs. differences)
1 1701  1                       : # of Sun angles, spectral channels; spectrum step
33.4.           : Sun zeniths
700. 571. 650. 838. 1677. 2217. : spectral channels (TM)
0. 2. 0. : view nadir angle, its increment, and view azimuth angle ***
!!! the following lines are not required for direct problem !!! ***
'powell'                                : name of the optimization subroutine
5000    1       100     100             : nfmax, itmax, itbr, nbrak
1.E-09  1.E-07  1.E-13  1.E-08          : zeps, tolbr, tiny, ftolp
1.      .5      2.      .2              : alpha, beta, gamma, dx
1       20.     f                       : n, at, lig - which initial guess
1       7                               : ll
486.    0.0211  0.0033  th_Sun=30.
572.    0.0332  0.0030  th_Sun=30.
661.    0.0162  0.0029  th_Sun=40.
838.    0.3441  0.0146  th_Sun=40.
1677.   0.1451  0.0073  th_Sun=45.
2217.   0.0498  0.0044  th_Sun=45.

****|****|****|****|****|****|****|****|****|****|****|****|****|****|****|****|
        rho     stdev
lambda  transmittance   reflectance
```

A.2 Reflectance Simulation Module

```
#!/usr/local/bin/perl

#-----------------------------------------------------------------
# mod1.pl
#
# This module
# - applies forest dynamic constraints to produce a new
#   basic input file
# - calls FRT to simulate canopy reflectanc for each
#   combination of free parameters
# - has H, FMC, NDM free
#
# Limitations:
# 1. The forest dynamics are only for Douglas-fir
# 2. The regression model for crown radius is for pine
#-----------------------------------------------------------------
#=================================================
# define index for a parameter, which is the same
# as the number at the last columne of input file
#=================================================

# SD
$sdNum = 1;

# H
$hNum = 2 ;

 # FMC
$fmcNum=13;

# crown length
$clNum=3;

# crown cylinder length
$cylNum=4;

# crown radius
$crNum=5;

# DBH
$dbhNum = 6;

# NDM
$ndmNum=7;

#  tree height, H
@HS = ("15","24","33","42","51");

# stem density, SD
@SDS = ("3781", "2002", "1016", "636", "433");

#-----------------------------------------------------------------
# coefficients for computing stand structural parameters
#-----------------------------------------------------------------
```

```
# for crown radius, m
$c1=0.1060;
$c2=0.6150;

# for crown length(cl, m)
$b1=-5.663;
$b2=0.683;
$b3=-0.0144;

# for computing DBH
@x = ("0", "0.000005", "0", "0", "0");
@y = ("-0.0026", "-0.0187", "-0.0197", "-0.0403","-0.0753");
@z = ("19.576", "35.881", "46.671", "63.396", "80.901");

#---------------------------------------------------------------------
# run the model for each scene with H, FMC and NDM free,
# and all other parameters are fixed
#---------------------------------------------------------------------
$basicInp='basicInput.txt';

$allOutFiles='>mod1/alloutfiles';
open(ALLOUTFILES,$allOutFiles);

# iterate over the free parameters and run
# FRT to simulate the top of canopy reflectance

# loop over H
for($k=1; $k<=5; ++$k){

   $H = @HS[$k-1];

   #loop over FMC
   for($i=1; $i<=1; ++$i){

      $FMC = 80 + 2*($i-1);

      #loop over NDM
      for($j=1; $j<=1;++$j){

         $NDM = 1+($j-1)*0.5;
         $SD = @SDS[$k-1];

         # compute DBH from SD based on the regression model for each H
         $DBH = @x[$k-1]*$SD*$SD + @y[$k-1]*$SD + @z[$k-1];

         # compute other parameters based on H and DBH
         # crown length
         $CL = $b1+$b2*$H+$b3*$DBH;

         # cylinder length
         $CYL = $H-$CL;

         # crown radius
         $D = $c1*$DBH+$c2*$DBH/$H;
         $CR = ($D/2);
```

```
#open the basic input file
open(FILE2, $basicInp) || die "cannot open file";

#new input file in this iteration
$inputfile = '>mod1/newInp.txt';
open(NEWFILE2,$inputfile) || die "cannot open new input file";

#find the line that contains a free parameter
while(<FILE2>) {

  $line=$_;

  # H
  if($line =~ /\s($hNum)$/) {
     print $line;
     @a=split(/\s+/,$line);
     @a[0]=$H;
     $line=join("     ",@a);
     print NEWFILE2 $line;
     print NEWFILE2 "\n";
  }
  # FMC
  elsif($line =~ /\s($fmcNum)$/) {
     print $line;
     @a=split(/\s+/,$line);
     @a[0]=$FMC;
     $line=join("     ",@a);
     print NEWFILE2 $line;
     print NEWFILE2 "\n";
  }
  # SD
  elsif($line =~ /\s($sdNum)$/){
     @a=split(/\s+/,$line);
     @a[0]=$SD*0.0001;
     $line=join("     ",@a);
     print NEWFILE2 $line;
     print NEWFILE2 "\n";
  }
  # DBH
  elsif($line =~ /\s($dbhNum)$/){
     @a=split(/\s+/,$line);
     @a[0]=$DBH;
     $line=join("     ",@a);
     print NEWFILE2 $line;
     print NEWFILE2 "\n";
  }
  # CL
  elsif($line =~ /\s($clNum)$/){
     @a=split(/\s+/,$line);
     @a[0]=$CL;
     $line=join("     ",@a);
     print NEWFILE2 $line;
     print NEWFILE2 "\n";

  }
  # CYL
```

```
            elsif($line =~ /\s($cylNum)$/){
               @a=split(/\s+/,$line);
               @a[0]=$CYL;
               $line=join("     ",@a);
               print NEWFILE2 $line;
               print NEWFILE2 "\n";
            }
            # CR
            elsif($line =~ /\s($crNum)$/){
               @a=split(/\s+/,$line);
               @a[0]=$CR;
               $line=join("     ",@a);
               print NEWFILE2 $line;
               print NEWFILE2 "\n";
            }
            # NDM
            elsif($line =~ /\s($ndmNum)$/){
               @a=split(/\s+/,$line);
               @a[0]=$NDM;
               $line=join("     ",@a);
               print NEWFILE2 $line;
               print NEWFILE2 "\n";
            }
            else{
               print NEWFILE2 $line; # echo line read
            }
         }

         close(FILE2);
         close(NEWFILE2);

         # submit job for running FRT model
         $ouFile="mod1/H"."$k"."_"."FMC"."$i"."_"."NDM"."$j";
         $inFile='mod1/newInp.txt';
         system "./frt $inFile $ouFile";

         #put all output file names into one file
         print ALLOUTFILES $ouFile;
         print ALLOUTFILES "\n";
      }
   }
}

close(ALLOUTFILES);
```

A.3 LUT Generation Module

```
%==========================================================
% lut.m
% - extracts simulated reflectance
% - integrates reflectance with 1 nm interval into AVIRIS-bands
% - produces LUT with H, FMC, LAI free
%
% @ author Jing Yang Li
% @ 2005/SEP/28
%==========================================================

format long;

% load FWHM
FWHM=load('AVIRIS2001_FWHM.txt');

s=size(FWHM);
num_aviris_bands=s(1);

% load Lambda
LAMBDA=load('AVIRIS2001_Lambda.txt');

% load modeled reflectance
ref=load('modeledReflectance.txt');
s=size(ref);

%number of simulations
num_simulations=s(1);

% ------------------------------------------------------------
% specify the bands you want to include in the LUT
%-------------------------------------------------------------

% by default, it includes all the bands from
% band 5 (412.69 nm) to band 212 (2388.80 nm)
lutBands = 5:212;

s=size(lutBands');
%number of bands in LUT
num_out_bands = s(1);

%loop over each simulation
for i = 1 : num_simulations,

   % get the first three column
   thisLut(i,1) = ref(i,1);
   thisLut(i,2) = ref(i,2);
   thisLut(i,3) = ref(i,3);

   %loop over each LUT band
   for j = lutBands(1) : lutBands(num_out_bands),

         % find the center band in the simulated reflectance
         for k=1:2001,
            if(abs(LAMBDA(j)-(399+k)) < 0.5)
```

```
            centerIndex = k;
            end
        end

        % compute the starting and ending index
        startIndex = centerIndex-10;
        endIndex   = centerIndex+10;

        % set parameters for Gaussian function
        sigma=FWHM(j)/(2*sqrt(2*log(2)));
        p2 = sqrt(2)*sigma;
        p1 = LAMBDA(j);

        totalf=0;
        totalr=0;

        % integrate
        for m = startIndex : endIndex,
            x = 399+m; % wavelength
            f = exp(-((x-p1)/p2).^2);
            totalf = totalf + f;
            totalr = totalr + f*ref(i,m+3);
        end

    thisLut(i,j-lutBands(1)+4) = totalr/totalf;

  end
end

% save the LUT
save('lutAll.txt','thisLut','-ascii','-double');
```

A.4 FMC Estimation Module

```
;This module generates a Fuel Moisture Content(FMC) map
;by using lookup table inversion method
;
;INPUT:
; 1. AVIRIS image
; 2. A 3-D lookup table
;
;OUTPUT:
; water content map
;
;AUTHOR: Jing Yang Li, 2005
;
;=============================================
; Function:
; check if a file is open
;=============================================
FUNCTION file_open_msg, para, message_text

   IF(SIZE(para, /TYPE) EQ 7) THEN BEGIN ;string type
      IF(para EQ '') THEN BEGIN ;empty string?
         result = DIALOG_MESSAGE(message_text,/INFORMATION)
         RETURN, -1
      ENDIF
   ENDIF

   IF(SIZE(para, /TYPE) EQ 3) THEN BEGIN ;longword integer type
      IF(para EQ -1) THEN BEGIN ;not valid fid
         result = DIALOG_MESSAGE(message_text,/INFORMATION)
         RETURN, -1
      ENDIF
   ENDIF

   RETURN, 0
END

;=============================================
; Function:
; computes the objective function
;=============================================
FUNCTION OBJ_FUNC,r_mea,r_mod

   obj = 0.0d
   sum = 0.0d

 ;weight for each band; you can experiment on the effect of different bands by giving it a weight
 w = [1.0,1.0,1.0]
;scale the simulated ref
s = [1.0,1.0,1.0]
for i=0,2 do begin
```

```
      tmp = r_mea[i]*s[i]-r_mod[i]
      sum = sum + w[i]*tmp*tmp
   endfor

   obj = sqrt(sum)
   return, obj
END

;=============================================================
; Function:
; searche the whole LUT to find the entry that
; best match the remotely sensed reflectance
;=============================================================
FUNCTION GLOBAL_SEARCH, lut, ref_measure,lutBands

   s1 = size(lut)
   n_water = s1[1]

   s2=size(ref_measure)
   n_bands=s2[1]
   ref_model=dblarr(n_bands)

   err=10.d
   i_water=-1;

   ;loop over all entries in the LUT
   for j=0,n_water-1 do begin

      ;get modeled ref. of this entry
      for i=0,n_bands-1 do begin
         ref_model[i]=lut[j,lutBands[i]+2]
      endfor

      ;compute objective function
      tmp = OBJ_FUNC(ref_measure,ref_model)

      if (tmp LT err) then begin
         err=tmp
         i_water=j
      endif

   endfor ;// end of j

   return, i_water
END

;=============================================================
; Function:
; searches the LUT locally to find the entry that
; best match the remotely sensed reflectance;
; the location center is determined by its spatial
; neighbor's entry in LUT
;=============================================================

FUNCTION LOCAL_SEARCH,lut,ref_measure,i_neighbor,lutBands
```

```
s1=size(lut)
n_water=s1[1]

s2=size(ref_measure)
n_bands=s2[1]

ref_model=dblarr(n_bands)

err=100.d

thresh=0.01d
;=============================
; set the local search range
;=============================

;2*nn+1 is the size of the local range
nn=10

;is: start index of the local range
is=i_neighbor - nn
if (is LT 0 ) then begin
   is=0
endif

;ie: end index of the local range
ie=i_neighbor + nn
if (ie GT n_water-1) then begin
   ie=n_water-1
endif

;=============================
; iterate over the local range
;=============================
for j=is,ie do begin

   ;get modeled ref. of this entry
   for i=0,n_bands-1 do begin
      ref_model[i]=lut[j,lutBands[i]+2]
   endfor

   ;compute merit function
   tmp = OBJ_FUNC(ref_measure,ref_model)

   if (tmp LT err) then begin
      err=tmp
      i_water=j
   endif

endfor ;// end of j

;the best match is not acceptable
if(err GT thresh) then begin
  i_water=-1
endif

return,i_water
```

```
END

pro waterMap, event

;=============================
; Function:
; selects image and mask file
;=============================
ENVI_SELECT, title='Input Filename', fid=fid, pos=pos,dims=dims, $
   /file_only,/no_dims,/no_spec,/mask, m_fid=m_fid, m_pos=m_pos

;check file ID
IF(file_open_msg(fid, 'Image file is not open!') EQ -1) THEN RETURN

;get file information from the header of the file
ENVI_FILE_QUERY, fid, data_type=data_type, xstart=xstart,ystart=ystart, $
   interleave=interleave, wl=wl,nb=nb,nl=nl,ns=ns,fwhm=fwhm,          $
   wavelength_unit=wu,sname=sname

;string for header comment if masked
s_mask=""

;default mask with all pixels switched on (same as no mask)
mask= MAKE_ARRAY(ns,nl,/BYTE, VALUE=1)

IF(m_pos GE 0) THEN BEGIN
   mask=ENVI_GET_DATA(dims=dims, fid=m_fid,pos=m_pos)
   ENVI_FILE_QUERY,m_fid,sname=mname
   s_mask += "masking it with " + mname + "and"
ENDIF

;print, size(mask)

IF( nb LE 2) THEN BEGIN
   ENVI_REPORT_ERROR, "The image " + sname +" contains insufficent bands to process."
ENDIF

!ORDER=1
b1=1 ;band number can be 0 to nb-1
data= ENVI_GET_DATA(fid=fid,dims=dims,pos=b1)
;print, size(data)
s=size(data);

NSAM=0L ;number of samples, x-direction
NSAM=s(1);
print,NSAM

NLIN=0L ;number of lines, y-direction
NLIN=s(2);
NBAN=204L ; number of bands

mr=data;
;tv,data
```

```
;=============================
;load LUT
;=============================
;3-D
nfree = 3   ;number of free dimensions
nband = 10  ;number of simulated bands
nwter = 3905;number of realizations of forest scene

array = dblarr(nband + nfree, nwter)
;infile= 'P:\thesis\mod3\lut302v1.txt'
infile = 'C:\Documents and Settings\jingli\My Documents\MyThesis\mod3\lut302v1.txt'
openr, inlun, infile, /get_lun
readf, inlun, array
close, inlun
free_lun, inlun

;revrese the array order
lut=transpose(array)

;Create a processing status report dialog
ENVI_REPORT_INIT, ['FMC mapping ...'], $
        title = 'Processing Status', base = base, /interupt
ENVI_REPORT_INC, base, 100

;=============================
;estimate FMC for each pixel
;=============================
nm = 3;number of bands used in merit function
lutBands = [6,8,10] ;index for band 903,1192, 1650nm

;measured reflectance at the water bands
ref_mea = dblarr(nm)-1.0

i_water = -1
i_neighbor = -1
water = dblarr(NSAM,NLIN)+0.d ; the array for storing retrieved water

;the index of water bands in this dataset
ind_903 =51;
ind_1192=81
ind_1650=108

;=========================
; iterate over each pixel
;=========================
for j=0,NLIN-1 do begin
  for i=0,NSAM-1 do begin

  ENVI_REPORT_STAT, base, j, NLIN-1      ;Update status report dialog
     ;only work on Douglas-fir dominant pixels
     if(mask[i,j] GE 14) then begin
        ;measured reflectance
        mr1 = ENVI_GET_DATA(fid=fid,dims=dims,pos=ind_903);
        mr2 = ENVI_GET_DATA(fid=fid,dims=dims,pos=ind_1192);
        mr3 = ENVI_GET_DATA(fid=fid,dims=dims,pos=ind_1650);
```

```
            ref_mea[0] = mr1[i,j]*0.0001
            ref_mea[1] = mr2[i,j]*0.0001
            ref_mea[2] = mr3[i,j]*0.0001

            ;if((r1 ne 0.0) and (r2 ne 0.0) and (r3 ne 0.0) and (r4 ne 0.0)) then begin
              if((ref_mea[0] gt 0.0) ) then begin

                  if(i_neighbor LT 0) then begin

                     ;find the index of the entry in LUT whose reflectance
                     ;best matches the measured reflectance
                     i_water = GLOBAL_SEARCH(lut,ref_mea,lutBands)
                     i_neighbor = i_water

                   endif else begin

                     ;do local serach
                     i_water = LOCAL_SEARCH(lut,ref_mea,i_neighbor,lutBands)

                     ;local search is not acceptable, so do a global search
                     if(i_water lt 0) then begin

                        ;print,'local search not good enough'
                        i_water = GLOBAL_SEARCH(lut,ref_mea,lutBands)
                        i_neighbor = i_water

                     endif else begin
                        ;print, 'GOOD local search'
                     endelse

                  endelse

                  ;set this pixel's water content
                  if(i_water GE 0) then begin
                     water[i,j] = lut[i_water,1]
                     print, water[i,j]
                  endif

               endif else begin
                  water[i,j] = 0
               endelse

     endif;//end of mask
   endfor;//end of i
endfor;//end of j

ENVI_REPORT_INIT, base = base, /finish ;Close status dialog
;============================
;output estimated FMC
;============================
;save estimated water map
openw,1,'C:\Documents and Settings\jingli\My Documents\MyThesis\mod3\FMC_d1s12.dat'
printf,1,water
close,1

END
```

A.5 Tutorial for running FMC estimation module

Assumptions:

LUT has been generated from the earlier experiments. AVIRIS image has been processed to reflectance and classified into forest species.

The steps to execute this module are as following.

1. Start ENVI. Then, in the IDL window, open the IDL program called watermap.pro.
2. Click the *Run* menu; click *Compile watermap.pro*; click *run watermap.pro*.
3. An *Input Filename* window will pop up.
4. Click *Open* and the select the image from *New File*. Do the same to select the mask.
5. In the *Select Input File* box choose the image.
6. Click *Select Mask Band.*
7. A *Select Mask Input Band* will pop up. Select the mask band. Click *OK*
8. Click *OK* in the *Input Filename* window. The program will run.
9. The FMC map will be created.